Mediterranean Sea Production Centre
MEDSEA_ANALYSISFORECAST_PHY_006_013

Issue: 2.2.1

Contributors: E. Clementi, A. Grandi, A.C. Goglio, A. Aydogdu, V. Lyubartsev, J. Pistoia, R. Escudier

Approval date by the CMEMS product quality coordination team:

CHANGE RECORD

When the quality of the products changes, the QuID is updated, and a row is added to this table. The third column specifies which sections or sub-sections have been updated. The fourth column should mention the version of the product to which the change applies.

Issue	Date	§	Description of Change	Author	Validated By
1.0	25-09-2017	All	Release of EAS2 version of the Med-Currents analysis and forecast product at 1/24° resolution	E. Clementi, A. Grandi, P. DiPietro, J. Pistoia, D. Delrosso, G. Mattia	E. Clementi (Med-MFC Deputy)
1.1	18-01-2018	All	Release of EAS3 version of the Med-Currents analysis and forecast product at 1/24° resolution	E. Clementi, A. Grandi, P. DiPietro, J. Pistoia, D. Delrosso, G. Mattia	E. Clementi (Med-MFC Deputy)
1.2	28-01-2019	All	Release of EAS4 version of the Med-Currents analysis and forecast product at 1/24° resolution	E. Clementi, A. Grandi, R. Escudier, V. Lyubartsev	E. Clementi (Med-MFC Deputy)
1.3	06-12-2019	All	Release of EAS5 version of the Med-Currents analysis and forecast product at 1/24° resolution	E. Clementi, A. Grandi, V. Lyubartsev	E. Clementi (Med-MFC Deputy)
1.4	10-09-2020	II.1 II.2 II.3 V	Use of higher resolution ECMWF atmospheric forcing	E. Clementi, A. Grandi, J. Pistoia	E. Clementi (Med-MFC Deputy)
2.0	15-01-2021	All	Updated document for the new product: modeling system including tides	E. Clementi, A. Grandi, A.C. Goglio, A. Aydogdu, J. Pistoia, V. Lyubartsev	E. Clementi (Med-MFC Deputy)

Issue	Date	§	Description of Change	Author	Validated By
2.1	10-09-2021	II, IV, V	Updated document for new upstream river data	E. Clementi, A. Grandi, A.C. Goglio	E. Clementi (Med-MFC Deputy)
2.2	01-12-2021	IV, V	Updated document for SST satellite upstream data change and delivery of updated timeseries	E. Clementi	E. Clementi (Med-MFC Deputy)
2.2.1	23-09-2022	III.4, V	Updated document for upstream data change: SLA Sentinel-6A assimilation	E. Clementi, A. Aydogdu, A. Grandi, A.C. Goglio	E. Clementi (Med-MFC Deputy)

TABLE OF CONTENTS

I   EXECUTIVE SUMMARY

I.1 Products covered by this document

The product covered by this document is the MEDSEA_ANALYSISFORECAST_PHY_006_013: the analysis and forecast nominal product of the physical component of the Mediterranean Sea with 1/24° (~4.5 km) horizontal resolution and 141 vertical levels.

The variables produced are:

- 3D daily, hourly and monthly mean fields of: Potential Temperature, Salinity, Zonal and Meridional Velocity
- 2D daily, hourly and monthly mean fields of: Sea Surface Height, Se Surface Zonal and Meridional Velocity, Mixed Layer Depth, Seabed Temperature (temperature of the deepest layer or level)
- 15 minutes instantaneous fields of: Sea Surface Height, Se Surface Zonal and Meridional Velocity

Product reference:

Clementi, E., Aydogdu, A., Goglio, A. C., Pistoia, J., Escudier, R., Drudi, M., Grandi, A., Mariani, A., Lyubartsev, V., Lecci, R., Cretí, S., Coppini, G., Masina, S., & Pinardi, N. (2021). Mediterranean Sea Analysis and Forecast (CMEMS MED-Currents, EAS6 system) (Version 1) [Data set]. Copernicus Monitoring Environment Marine Service (CMEMS).
https://doi.org/10.25423/CMCC/MEDSEA_ANALYSISFORECAST_PHY_006_013_EAS6

I.2 Summary of the results

The quality of the MEDSEA_ANALYSISFORECAST_PHY_006_013 analysis and forecast product provided by the EAS6 modelling system, is assessed over 1 year period from 01/01/2019 to 31/12/2019 by means of temperature, salinity, sea level anomaly, sea surface height, currents, seabed temperature and mixed layer depth using independent (for surface currents), quasi-independent satellite and in-situ observations, climatological datasets as well as the inter-comparison with the previous version of the MEDSEA_ANALYSISFORECAST_PHY_006_013 product timeseries corresponding to the EAS5 modelling system.

The main results of the MEDSEA_ANALYSISFORECAST_PHY_006_013 quality assessment are summarized below:

Sea Surface Height: the EAS6 system presents a slightly better accuracy in terms of sea surface height representation with respect to the previous version. The quality of the predicted SLA has been assessed by considering the RMS differences between the model daily outputs and the satellite along track observations, which is in average 3.6 cm. The new system presents a slightly decreased error with respect to the previous one (3.7 cm). Moreover, the harmonic analysis shows that the model has a high skill in representing tidal amplitudes and phases of all the considered tidal constituents, with larger error for the higher tidal amplitudes.

Temperature: the temperature is accurate with an error below 0.81°C when comparing to vertical in-situ observations at surface and below, and 0.76°C when comparing SST to satellite L4 dataset. The accuracy of the temperature along the water column presents higher RMS differences at first layers, which decreases below 60 m. Considering the SST, the RMS differences with respect to satellite observations vary in different subbasins, ranging from 0.47°C to 0.76°C. The MED-Currents products usually have a warm SST bias.

Salinity: the salinity is accurate with RMSD values lower than 0.18 PSU. The error is higher in the upper layers and decreases significantly below 150 m.

Currents: Surface currents RMSD and bias are evaluated against moored buoys. Due to the reduced number of observations, mainly located in coastal areas, the statistical relevance of currents performance is poor. In addition to the surface currents validation assessment, a derived validation assessment is provided in terms of transport at Straits including the net, eastward and westward transport through the Strait of Gibraltar showing a good agreement with literature values.

Bottom temperature: the bottom temperature of EAS6 system has been compared to SeaDataNet monthly climatology showing a good skill in representing the seasonal variability of the temperature at deepest level and a general overestimation with respect to the climatological dataset. The spatial pattern of the seabed temperature is correctly represented by the system

Mixed Layer Depth: the MLD in the EAS6 system has been compared to climatological estimates from literature (Houpert at al., 2015) showing that the model is able to correctly represent the depth of the mixed layer with spatial and seasonal differences. In general, it can be noticed that the main differences could arise due to the low resolution of the climatological dataset that, moreover, do not cover the whole domain of the Mediterranean Sea.

I.3 Estimated Accuracy Numbers

Estimated Accuracy Numbers (EANs), that are the mean and the RMS of the difference between the model and in-situ or satellite reference observations, are provided in the following table.

EAN are computed for:

- Temperature;
- Salinity;
- Sea Surface Temperature (SST);
- Sea Level Anomaly (SLA).

The observations used are:

- vertical profiles of temperature and salinity from Argo floats and XBTs (if available): INSITU_MED_TS_NRT_OBSERVATIONS_013_035

- SST satellite data from CMEMS SST-TAC product:

  SST_MED_SST_L4_NRT_OBSERVATIONS_010_004, SST_MED_SST_L3S_NRT_OBSERVATIONS_010_012

- Satellite Sea Level along track data from CMEMS SL-TAC product:

  SEALEVEL_EUR_PHY_L3_REP_OBSERVATIONS_008_061, SEALEVEL_EUR_PHY_L3_NRT_OBSERVATIONS_008_059

The EANs are evaluated for the EAS6 system over 1 year period from January to December 2019 and are computed for the whole Mediterranean Sea and its 16 sub-regions Figure 1: (1) Alboran Sea, (2) South West Med 1 (western part), (3) North West Med, (4) South West Med 2 (eastern part), (5) Tyrrhenian Sea 2 (southern part), (6) Tyrrhenian Sea 1 (northern part), (7) Ionian Sea 1 (western part), (8) Ionian Sea 2 (south-eastern part), (9) Ionian Sea 2 (north-eastern part), (10) Adriatic Sea 2 (southern part), (11)

Adriatic Sea 1 (northern part), (12) Levantine Sea 1 (western part), (13) Aegean Sea, (14) Levantine Sea 2 (central-northern part), (15) Levantine Sea 3 (central southern part), (16) Levantine Sea 4 (eastern part).
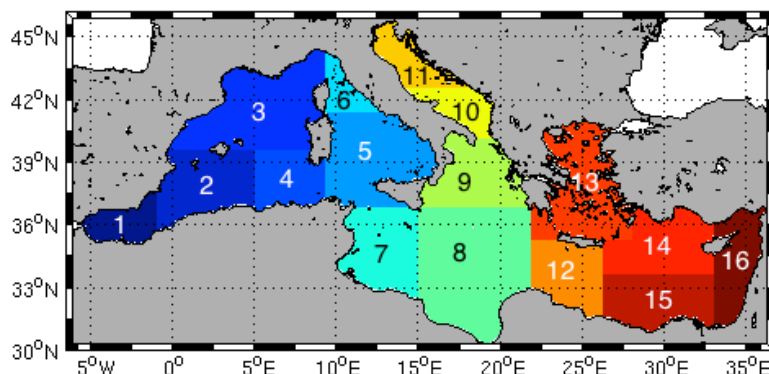
Figure 1. The Mediterranean Sea sub-regions subdivision for validation metrics

The EANs of temperature and salinity are then evaluated at 9 different layers: 0-10, 10-30, 30-60, 60-100, 100-150, 150-300, 300-600, 600-1000, 1000-2000 [m] in order to better verify the model ability to represent the vertical structure of the temperature and salinity fields.

In the following tables the EANs corresponding to Mean (Observations minus Model) and RMSD for the EAS6 system are presented.

T prod – T ref [°C]	EAS6 system	
Layer (m)	Mean (Obs-Model)	RMSD
0-10	-0.04	0.56
10-30	-0.04	0.81
30-60	0.03	0.81
60-100	0.03	0.52
100-150	0.01	0.36
150-300	-0.01	0.30
300-600	-0.01	0.20
600-1000	0.02	0.09
1000-2000	0.02	0.05

Table 1: The EANs of temperature at different vertical layers evaluated for the EAS6 system for the year 2019

SST prod – SST ref [°C]	EAS6 system

REGION	Mean (Obs-Model)	RMSD
MED SEA	0.14	0.57
REGION 1	-0.20	0.74
REGION 2	0.14	0.57
REGION 3	-0.04	0.57
REGION 4	0.27	0.76
REGION 5	0.1	0.48
REGION 6	0.15	0.47
REGION 7	0.22	0.52
REGION 8	0.22	0.58
REGION 9	0.17	0.52
REGION 10	0.15	0.55
REGION 11	-0.02	0.61
REGION 12	0.05	0.49
REGION 13	0.17	0.61
REGION 14	0.16	0.55
REGION 15	0.18	0.56
REGION 16	0.32	0.58

Table 2: The EANs of Sea Surface Temperature evaluated for the EAS6 system for the year 2019 for the Mediterranean Sea and 16 regions (see Figure 1).

S prod – S ref [PSU]	EAS6 system	
Layer (m)	Mean (Obs-Model)	RMSD
0-10	0.01	0.17
10-30	0.00	0.18
30-60	-0.01	0.17
60-100	-0.01	0.15
100-150	-0.01	0.12
150-300	0.00	0.08
300-600	-0.01	0.05
600-1000	0.00	0.03
1000-2000	0.00	0.02

Table 3: The EANs of salinity at different vertical layers evaluated for the EAS6 system for year 2019.

SLA prod – SLA ref [cm]	EAS5 system	EAS56 system

REGION	RMSD	RMSD
MED SEA	3.7	3.6
REGION 1	6.1	4.8
REGION 2	4.2	4.2
REGION 3	3.2	3.4
REGION 4	5.0	5.2
REGION 5	3.2	3.1
REGION 6	3.3	3.3
REGION 7	3.3	3.3
REGION 8	3.4	3.3
REGION 9	3.3	3.1
REGION 10	2.6	2.6
REGION 11	2.7	2.7
REGION 12	4.1	3.9
REGION 13	4.4	4.4
REGION 14	3.2	3.1
REGION 15	4.0	3.9
REGION 16	3.5	3.4

Table 4: The EANs of Sea Level Anomaly evaluated for the EAS5 and EAS6 systems for year 2019 for the Mediterranean Sea and 16 sub-regions (see Figure 1).

The metrics of Table 1 and Table 2 give indications about the accuracy of MEDSEA_ANALYSISFORECAST_PHY_006_013 temperature variable along the water column and at the surface for the Mediterranean Sea and 16 sub-regions. The values for all the vertical levels are computed using Argo profiles while the SST is evaluated by comparing with satellite observations. The temperature RMSD and MEAN values are higher at the first levels and decrease significantly below the fourth layer. The RMSD is always lower than 0.81°C along the water column, while it ranges between 0.48 and 0.76°C for the SST.

The statistics listed in Table 3 give indications about the accuracy of the MEDSEA_ANALYSISFORECAST_PHY_006_013 salinity field. The values for all the levels are computed using Argo profiles. The system presents a RMSD always lower than 0.18 PSU with higher error at the surface which decreases below 150 m.

The metrics shown in Table 4 define the accuracy of MEDSEA_ANALYSISFORECAST_PHY_006_013 sea level anomaly. The statistics are computed along the satellite tracks. The new system presents an overall RMS difference of 3.6 cm in the whole basin, while it ranges between 2.6 and 5.2 cm in the different regions.

II   PRODUCTION SYSTEM DESCRIPTION

Production centre name: CMCC

Production system name: Analysis and Forecast Med-Currents EAS6 system

CMEMS Product name: MEDSEA_ANALYSISFORECAST_PHY_006_013

External product: Temperature (3D), Salinity (3D), Meridional and Zonal Currents (3D), Sea Surface Height (2D), Mixed Layer Depth (2D), Seabed Temperature (2D)

Frequency of model output: daily (24-hrs) averages, hourly (1-hr) averages, monthly averages, 15 min instantaneous fields

Geographical coverage: -17.2917°W → 36.29167°E; 30.1875°N → 45.97917°N (Bay of Biscay and Black Sea are excluded)

Horizontal resolution: 1/24°

Vertical coverage: From surface to 5754 m (141 vertical unevenly spaced levels).

Length of forecast: 10 days for the daily mean fields, 5 days for the hourly mean fields.

Frequency of forecast release: Daily.

Analyses: Yes.

Hindcast: Yes.

Frequency of analysis release: Weekly on Tuesday.

Frequency of hindcast release: Daily.

The analyses and forecasts physical product of the Med-MFC is produced with two different cycles: a daily cycle for the production of forecast, and a weekly cycle for the production of analysis.

The daily cycle is done each day (J), for the next 10 days. The forecast is initialized by a hindcast every day except Tuesday, when the analysis is used instead of the hindcast. Every day the product is updated with a hindcast for day J-1 and 10-day forecast.

The weekly cycle is done on Tuesday, for the previous 15 days. The assimilation cycle is daily (24hr) and is done in filter mode. Every Wednesday the product is updated with the analyses from day J-15 to day J-2, a hindcast for day J-1 and 10-day forecast.

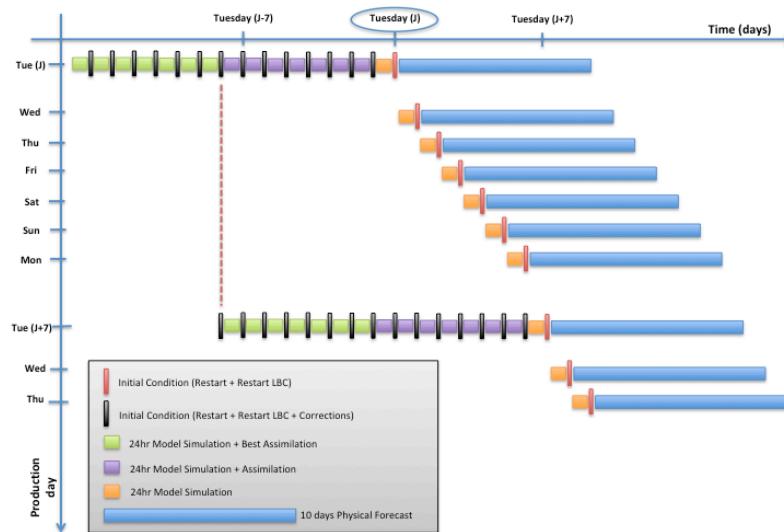The production chain is illustrated in Figure 2.

Figure 2: Scheme of the analysis and forecast CMEMS Med-Currents processing chain.

The Med-Currents system run is composed by several steps:

1. Upstream Data Acquisition, Pre-Processing and Control of: ECMWF atmospheric forcing (Numerical Weather Prediction), Satellite (SLA and SST) and in-situ (T and S) observations.

2. Forecast/Hindcast: NEMO-WW3 modelling system is run to produce one day of hindcast and a 10-day forecast.

3. Analysis/Hindcast (only on Tuesday): NEMO-WW3 modelling system is coupled with OceanVar, a 3Dvar assimilation scheme, in order to produce the best estimation of the sea (i.e. analysis). The NEMO+WW3+OceanVar system is running for 15 days into the past in order to use the best available along track SLA products. The latest day of the 15 days of analysis, produces the initial condition for the 10-day forecast.

4. Post processing: the model output is processed in order to obtain the products for the CMEMS catalogue.

5. Output Delivery.

II.1 Description of the Med-Currents EAS6 model system

The Mediterranean Forecasting System, MFS, (Pinardi et al., 2003, Pinardi and Coppini 2010, Tonani et al., 2014) is providing, since year 2000, analysis and short-term forecast of the main physical parameters in the Mediterranean Sea and it is the physical component of the Med-MFC called Med-Currents.

The analysis and forecast Med-Currents system at CMEMS EAS6 is provided by means of a coupled hydrodynamic-wave model implemented over the whole Mediterranean basin and extended into the Atlantic Sea in order to better resolve the exchanges with the Atlantic Ocean at the Strait of Gibraltar. The model horizontal grid resolution is 1/24˚ (ca. 4.5 km) and has 141 unevenly spaced vertical levels.

The hydrodynamics are supplied by the Nucleous for European Modelling of the Ocean (NEMO v3.6) while the wave component is provided by WaveWatch-III. The model solution is analysed and updated by OceanVar (an ocean 3Dvar scheme) assimilating temperature and salinity vertical profiles and along track satellite sea level anomaly observations.

Circulation model component (NEMO)

The oceanic equations of motion of Med-currents system are solved by an Ocean General Circulation Model (OGCM) based on NEMO (Nucleus for European Modelling of the Ocean) version 3.6 (Madec et al., 2019). The code is developed and maintained by the NEMO-consortium.

NEMO has been implemented in the Mediterranean at 1/24° x 1/24° horizontal resolution and 141 unevenly spaced vertical levels (Clementi et al., 2017a) with time step of 120 s. The model covers the whole Mediterranean Sea and also extends into the Atlantic in order to better resolve the exchanges with the Atlantic Ocean at the Strait of Gibraltar.

The NEMO code solves the primitive equations using the time-splitting technique that is the external gravity waves are explicitly resolved with non-linear free surface formulation and time-varying vertical z-star coordinates.

The advection scheme for active tracers, temperature and salinity, is a mixed up-stream/MUSCL (Monotonic Upwind Scheme for Conservation Laws; Van Leer, 1979), originally implemented by Estubier and Lévy (2000) and modified by Oddo et al. (2009). The vertical diffusion and viscosity terms are a function of the Richardson number as parameterized by Pacanowsky and Philander (1981).

The model interactively computes air-surface fluxes of momentum, mass, and heat. The bulk formulae implemented are described in Pettenuzzo et al. (2010) and are currently used in the Mediterranean operational system (Tonani et al., 2015). A detailed description of other specific features of the model implementation can be found in Oddo et al., (2009, 2014).

The vertical background viscosity and diffusivity values are set to 1.2e-6 [m^2/s] and 1.0e-7 [m^2/s] respectively, while the horizontal bilaplacian eddy diffusivity and viscosity are set respectively equal to -1.2e8 [m^4/s] and -2.0e8 [m^4/s]. A quadratic bottom drag coefficient with a logarithmic formulation has been used according to Maraldi et al. (2013) and the model uses vertical partial cells to fit the bottom depth shape.

Tidal waves have been included in the EAS6 system, so that the tidal potential is calculated across the domain for the 8 major constituents of the Mediterranean Sea: M2, S2, N2, K2, K1, O1, P1, Q1. In addition, tidal forcing is applied along the lateral boundaries in the Atlantic Ocean by means of tidal elevation estimated using FES2014 (Carrere et al., 2016) tidal model and tidal currents evaluated using TUGO (Toulouse Unstructured Grid Ocean model, ex-Mog2D, Lynch and Gray 1979).

The hydrodynamic model is nested in the Atlantic within the Global analysis and forecast system GLO-MFC daily data set (1/12° horizontal resolution, 50 vertical levels) that is interpolated onto the Med-Currents model grid. Details on the nesting technique and major impacts on the model results are in Oddo et al., (2009).

The model is forced by momentum, water and heat fluxes interactively computed by bulk formulae using the 1/10° horizontal-resolution operational analysis and forecast fields from the European Centre for Medium-Range Weather Forecasts (ECMWF) at highest available time frequency (1 hour for the first 3 days of forecast, 3 hours for the following 3 days of forecast and 6 hours for the last 4 days of forecast and for the analysis) and the model sea surface temperature (details of the air-sea physics are in Tonani et al., 2008). The water balance is computed as Evaporation minus Precipitation and Runoff. The evaporation is derived from the latent heat flux, precipitation is provided by ECMWF as daily averages, while the runoff of the 39 rivers implemented is provided by:

*) daily mean observed discharge for the Po river distributed by ARPAE (Regional Agency for Prevention, Environment and Energy of Emilia-Romagna, Italy) and available from the website: https://simc.arpae.it/dext3r/. The Po river discharge is measured at the closing point of the drainage basin in Pontelagoscuro.

*) monthly mean datasets for the remaining 38 rivers: the Global Runoff Data Centre dataset (Fekete et al., 1999) for the Ebro, Nile and Rhone rivers; the dataset from Raicich (1996) for: Vjosë, Seman rivers; the UNEP-MAP dataset (Implications of Climate Change for the Albanian Coast, Mediterranean Action Plan, MAP Technical Reports Series No.98., 1996) for the Buna/Bojana river; the PERSEUS dataset for the following 32 rivers: Piave, Tagliamento, Soca/Isonzo, Livenza, Brenta-Bacchiglione, Adige, Lika, Reno, Krka, Arno, Nerveta, Aude, Trebisjnica, Tevere/Tiber, Mati, Volturno, Shkumbini, Struma/Strymonas, Meric/Evros/Maritsa, Axios/Vadar, Arachtos, Pinios, Acheloos, Gediz, Buyuk Menderes, Kopru, Manavgat, Seyhan, Ceyhan, Gosku, Medjerda, Asi/Orontes.

Objective Analyses-Sea Surface Temperature (OA-SST) fields from CNR-ISA SST-TAC are used for the correction of surface heat fluxes with the relaxation constant of 110 $Wm^{-2}K^{-1}$ centered at midnight since the observed dataset corresponds to the foundation SST (~SST at midnight).

The Dardanelles Strait is implemented as a lateral open boundary condition by using GLO-MFC daily Analysis and Forecast product and daily climatology derived from a Marmara Sea box model (Maderich et al., 2015).

The topography is created starting from the GEBCO 30arc-second grid (http://www.gebco.net/data_and_products/gridded_bathymetry_data/gebco_30_second_grid/), filtered (using a Shapiro filter) and manually modified in critical areas such as: islands along the Eastern Adriatic coasts, Gibraltar and Messina straits, Atlantic box edge.

Wave model component (WW3)

The wave dynamic is solved by a Mediterranean implementation of the WaveWatch-III (WW3) code version 3.14 (Tolman, 2009). WaveWatch covers the same domain and follows the same horizontal discretization of the circulation model (1/24° x 1/24°) with a time step of 240 sec. The wave model uses 24 directional bins (15° directional resolution) and 30 frequency bins (ranging between 0.05 Hz and 0.7931 Hz) to represent the wave spectral distribution.

WW3 has been forced by the same 1/10° horizontal resolution ECMWF atmospheric forcing (the same used to force the hydrodynamic model). The wind speed is then modified by considering a stability parameter depending on the air-sea temperature difference according to Tolman (2002).

The wave model takes into consideration the surface currents for wave refraction but assumes no interactions with the ocean bottom. WW3 model solves the wave action balance equation that describes the evolution, in slowly varying depth domain and currents, of a 2D ocean wave spectrum where individual spectral component satisfies locally the linear wave theory. In the present application WW3 has been implemented following WAM cycle4 model physics (Gunther et al., 1993). Wind input and

dissipation terms are based on Janssen's quasi-linear theory of wind-wave generation (Janssen, 1989, 1991). The dissipation term is based on Hasselmann (1974) whitecapping theory according to Komen et al. (1984). The non-linear wave-wave interaction is modelled using the Discrete Interaction Approximation (DIA, Hasselmann et al., 1985).

Model coupling (NEMO-WW3)

The coupling between the hydrodynamic model (NEMO) and the wave model (WW3) is achieved by an online hourly two-way coupling and consists in exchanging the following fields: NEMO sends to WW3 the air-sea temperature difference and the surface currents, while WW3 sends to NEMO the neutral drag coefficient used to evaluate the surface wind stress.

More details on the model coupling and on the impact of coupled system on both wave and circulation fields can be found in Clementi et al., (2017b).

Data assimilation scheme (OceanVar)

The data assimilation system is based on a 3D variational ocean data assimilation scheme, OceanVar, developed by Dobricic and Pinardi (2008) and later upgraded by Storto et al. (2015). The background error covariance matrices vary monthly at each grid point in the discretized domain of the Mediterranean Sea. EOFs have been calculated from a three-years long simulation (in the future EOFs will be updated using the new long-term reanalysis product). The observations that are assimilated are: along-track sea level anomaly (a satellite product including dynamical atmospheric correction and ocean tides is chosen, as specified in II.3) from CLS SEALEVEL-TAC, and in-situ vertical temperature and salinity profiles from VOS XBTs (Voluntary Observing Ship-eXpandable Bathythermograph) and ARGO floats. In-situ observational errors are estimated iteratively as described in Desroziers et al. (2005). The altimeter observation errors are assumed to be the same for all satellites and is 3 cm. The misfits with the observations (innovations) are computed with the First Guess at Appropriate Time (FGAT) technique.

II.2 New features of the Med-Currents EAS6 system

The main differences between the CMEMS Med-Currents EAS5 and EAS6 systems are summarized in Table 5 and described hereafter.

	CMEMS Med-Currents EAS6
Upgrades in the modelling system	Inclusion of tides: the tidal potential is calculated across the domain for the 8 major constituents of the Mediterranean Sea: M2, S2, N2, K2, K1, O1, P1, Q1. In addition to this, tidal forcing is applied along the lateral boundaries in the Atlantic Ocean by means of tidal elevation and tidal currents. Reduction of the NEMO time step from 240 to 120 sec. Change of model bathymetry. Increased bottom friction at Gibraltar strait.
Changes in Data Assimilation	The altimeter observation errors are assumed to be the same for all satellites and is set 3 cm (instead of 4 cm as in the previous system). Accounting the tidal signal in the altimeter tracks.
New variables in catalogue	Added 15 minutes instantaneous SSH, SSU, SSV fields. Added SSH detided fields removing from model SSH the tidal signal evaluated using TPXO (barotropic tidal model).

Table 5: Differences between CMEMS Med-Currents EAS6 system and the previous one (EAS5).

II.3 Upstream data and boundary condition of the NEMO-WW3-OceanVar system

The CMEMS MED-Currents system uses the following upstream data:

1. Atmospheric forcing (including precipitation): NWP 6-h (1-h for the first 3 days of forecast, 3-h for the following 3 days of forecast), 0.10° horizontal-resolution operational analysis and forecast fields from the European Centre for Medium-Range Weather Forecasts (ECMWF) distributed by the Italian National Meteo Service (USAM/CNMA)

2. Runoff: ARPAE (Regional Agency for Prevention, Environment and Energy of Emilia-Romagna, Italy, https://simc.arpae.it/dext3r/) daily measurements for the Po river; Monthly climatologies derived from: Global Runoff Data Centre dataset (Fekete et al., 1999) for Ebro, Nile and Rhone, the dataset from Raicich (Raicich, 1996) for the Adriatic rivers Vjosë and Seman; the UNEP-MAP dataset (Implications of Climate Change for the Albanian Coast, Mediterranean Action Plan, MAP Technical Reports Series No.98., 1996) for the Buna/Bojana river; the PERSEUS project dataset for the new 32 rivers added.

3. Initial conditions of temperature and salinity at 1/1/2015 are the winter climatological fields from WOA13 V2 (World Ocean Atlas 2013 V2, https://www.nodc.noaa.gov/OC5/woa13/woa13data.html)

4. Lateral boundary conditions from CMEMS Global Analysis and Forecast system: GLOBAL_ANALYSISFORECAST_PHY_001_024 at 1/12° horizontal resolution, 50 vertical levels.

5. Lateral boundary tidal signal: tidal elevation from FES2014 (Carrere et al., 2016) and tidal currents from TUGO (Toulouse Unstructured Grid Ocean model, ex-Mog2D, Lynch and Gray 1979).

6. Data assimilation:

   o Temperature and Salinity vertical profiles from CMEMS INSITU TAC

     ▪ INSITU_MED_NRT_OBSERVATIONS_013_035

   o Satellite along track Sea Level Anomaly from CMEMS SL TAC:

     ▪ SEALEVEL_EUR_PHY_L3_REP_OBSERVATIONS_008_061 (until May 2019)

     ▪ SEALEVEL_EUR_PHY_L3_NRT_OBSERVATIONS_008_059 (from May 2019 to present)

   o Satellite SST from CMEMS SST TAC (nudging):

     ▪ SST_MED_SST_L4_NRT_OBSERVATIONS_010_004

III VALIDATION FRAMEWORK

In order to evaluate and assure the quality of the MEDSEA_ANALYSISFORECAST_PHY_006_013 product, an assimilation experiment has been performed using the system described in section II, which is going to be operational starting in May 2021, and covering 4 years from January 2015 to December 2019 (the period from January to December 2015 is considered as a spin-up and performed without assimilation).

In particular, the qualification task has been carried out over 1 year period, from January to December 2019, based on Class 1, Class2 and 4 diagnostics.

The performance of the Med-Currents EAS6 new system has been assessed by using external products: quasi-independent satellite and in-situ observations have been used to assess the skill of temperature, salinity and sea level anomaly; independent fixed moorings have been used to qualify coastal currents; independent tide gauges have been used to perform the harmonic analysis, moreover, climatological datasets have been used to assess the quality of the seabed temperature and mixed layer depth.

Quasi-independent data are all the observations (Satellite SLA and SST and in situ vertical profiles of temperature and salinity from XBT and Argo) which are assimilated into the system. Diagnostic in terms of RMS of the misfits and/or bias are computed using the model fields before the ingestion of the observations and applying the increments.

The datasets of observations used for the qualification task are listed below in Table 6 presenting the lists of the independent and quasi-independent datasets with the corresponding product names.

QUASI-INDEPENDENT DATA	
TYPE	**CMEMS PRODUCT NAME**
ARGO, XBT	INSITU_MED_NRT_OBSERVATIONS_013_035
SLA	SEALEVEL_EUR_PHY_L3_REP_OBSERVATIONS_008_061
	SEALEVEL_EUR_PHY_L3_NRT_OBSERVATIONS_008_059
SST	SST_MED_SST_L4_NRT_OBSERVATIONS_010_004
INDEPENDENT DATA	
TYPE	**PRODUCT NAME**
MOORINGS, Tide gauges	INSITU_MED_NRT_OBSERVATIONS_013_035
	EMODNET Physics

Table 6: list of the quasi-independent and independent observations

In this section the results of the validation task are presented in terms of: Temperature (including SST), Sea Bottom Temperature, Salinity, Sea Level Anomaly, Sea Surface Height, Currents (also in terms of transport at straits), and Mixed Layer Depth.

The list of metrics used to provide an overall assessment of the product, to quantify the differences with the available observations is presented in Table 7.

Name	Description	Ocean parameter	Supporting reference dataset	Quantity
NRT evaluation of Med-MFC-Currents using semi-independent data: Estimate Accuracy Numbers				
T-<X-Y>m-D-CLASS4-PROF-RMSD-Jan2019-Dec2019	Temperature vertical profiles comparison with CMEMS INSITU TAC data at several layers for the Mediterranean basin.	Temperature	Argo floats from the CMEMS INSITU TAC product: INSITU_MED_NRT_OBSERVATIONS_013_035	Time series of Temperature daily RMSs of the difference between model and insitu observations averaged over the qualification testing period (Jan-Dec 2019). This quantity is evaluated on the model analysis. The statistics are defined for all the Mediterranean Sea and are evaluated for several layers. Together with the time series, the time (2019) average RMSD value is reported in tables.
T-<X-Y>m-D-CLASS4-PROF-BIAS-Jan2019-Dec2019	Temperature vertical profiles comparison with CMEMS INSITU TAC data at several layers for the Mediterranean basin.	Temperature	Argo floats from the CMEMS INSITU TAC product: INSITU_MED_NRT_OBSERVATIONS_013_035	Time series of Temperature daily mean differences between model and insitu observations averaged over the qualification testing period (Jan-Dec 2019). This quantity is evaluated on the model analysis. The statistics are defined for all the Mediterranean Sea and are evaluated for several different layers. Together with the time series, the time (2019) averaged BIAS value is reported in tables.
S-<X-Y>m-D-CLASS4-PROF-RMSD-Jan2019-Dec2019	Salinity vertical profiles comparison with CMEMS INSITU TAC data at several layers for the Mediterranean basin.	Salinity	Argo floats from the CMEMS INSITU TAC product: INSITU_MED_NRT_OBSERVATIONS_013_035	Time series of Salinity daily RMSs of the difference between model and insitu observations averaged over the qualification testing period (Jan-Dec 2019). This quantity is evaluated on the model analysis. The statistics are defined for all the Mediterranean Sea and are evaluated for several different layers. Together with the time series, the time (2019) averaged RMSD value is reported in tables.
S-<X-Y>m-D-CLASS4-PROF-BIAS-Jan2019-Dec2019	Salinity vertical profiles comparison with CMEMS INSITU TAC data at several layers for the Mediterranean basin.	Salinity	Argo floats from the CMEMS INSITU TAC product: INSITU_MED_NRT_OBSERVATIONS_013_035	Time series of Salinity daily mean differences between model and insitu observations averaged over the qualification testing period (Jan-Dec 2019). This quantity is evaluated on the model analysis. The statistics are defined for all the Mediterranean Sea and are evaluated for several layers. Together with the time series, the time (2019) averaged BIAS value is reported in tables.

Table 7: List of metrics for Med-Currents evaluation using in-situ and satellite observations (continues in next pages).

Name	Description	Ocean parameter	Supporting reference dataset	Quantity
SLA-D-CLASS4-ALT-RMSD-Jan2019-Dec2019	Sea level anomaly comparison with CMEMS Sea Level TAC (satellite along track) data for the Mediterranean basin and selected sub-basins.	Sea Level Anomaly	Satellite Sea Level along track data from CMEMS Sea Level TAC product: SEALEVEL_EUR_PHY_L3_REP_OBSERVATIONS_008_061 SEALEVEL_EUR_PHY_L3_NRT_OBSERVATIONS_008_059	Time series of Sea level daily RMSs of the difference between model and satellite observations averaged over the qualification testing period (Jan-Dec 2019). This quantity is evaluated on the model analysis. The statistics are defined for all the Mediterranean Sea and 16 selected sub-basins. Together with the time series, the time (2019) average RMSD value is reported in tables.
SST-D-CLASS4-RAD-RMSD-Jan2019-Dec2019	Sea Surface Temperature comparison with SST CMEMS SST TAC L4 (satellite) data for the Mediterranean basin and selected sub-basins.	Sea Surface Temperature	SST satellite data from CMEMS SST TAC L4 product: SST_MED_SST_L4_NRT_OBSERVATIONS_010_004	Time series of Sea surface temperature daily RMSs of the difference between model and satellite observations averaged over the qualification testing period (Jan-Dec 2019). This quantity is evaluated on the model analysis. The statistics are defined for all the Mediterranean Sea and 16 selected sub-basins. Together with the time series, the time (2019) average RMSD value is reported in tables.
SST-D-CLASS4-RAD-BIAS-Jan2019-Dec2019	Sea Surface Temperature comparison with SST CMEMS SST TAC L4 (satellite) data for the Mediterranean basin and selected sub-basins.	Sea Surface Temperature	SST satellite data from CMEMS SST TAC L4 product: SST_MED_SST_L4_NRT_OBSERVATIONS_010_004	Time series of Sea surface temperature daily mean differences between model and satellite observations averaged over the qualification testing period (Jan-Dec 2019). This quantity is evaluated on the model analysis. The statistics are defined for all the Mediterranean Sea and 16 selected sub-basins. Together with the time series, the time (2019) average BIAS value is reported in tables.

Name	Description	Ocean parameter	Supporting reference dataset	Quantity
NRT evaluation of Med-MFC-Currents using semi-independent data. Weekly comparison of misfits				
T-<X-Y>m-W-CLASS4–PROF-RMSD-MED-Jan2019-Dec2019	Temperature vertical profiles comparison with assimilated CMEMS INSITU TAC data at 5 specified depths.	Temperature	Argo floats and XBT from the CMEMS INSITU TAC products: INSITU_MED_NRT_OBSERVATIONS_013_035	Time series of weekly RMSs of temperature misfits (observation minus model value transformed at the observation location and time). Together with the time series, the average value of weekly RMSs is evaluated over the qualification testing period (2019). The statistics are defined for all the Mediterranean Sea and are evaluated at five different depths: 8, 30, 150, 300 and 600 m.
S-<X-Y>m-W-CLASS4–PROF-RMSD-MED-Jan2019-Dec2019	Salinity vertical profiles comparison with assimilated CMEMS INSITU TAC data at 5 specified depths.	Salinity	Argo floats from the CMEMS INSITU TAC products: INSITU_MED_NRT_OBSERVATIONS_013_035	Time series of weekly RMSs of salinity misfits (observation minus model value transformed at the observation location and time). Together with the time series, the average value of weekly RMSs is evaluated over the qualification testing period (2019). The statistics are defined for all the Mediterranean Sea and are evaluated at five different depths: 8, 30, 150, 300 and 600 m.
SLA-SURF-W-CLASS4-ALT-RMSD-MED-Jan2019-Dec2019	Sea level anomaly comparison with assimilated CMEMS Sea Level TAC satellite along track data for the Mediterranean basin.	Sea Level Anomaly	Satellites (Jason2, Jason2N, Jason3, CryoSat-2, Saral/Altika, Sentinel3) Sea Level along track data from CMEMS Sea Level TAC products: SEALEVEL_EUR_PHY_L3_REP_OBSERVATIONS_008_061 SEALEVEL_EUR_PHY_L3_NRT_OBSERVATIONS_008_059	Time series of weekly RMSs of sea level anomaly misfits (observation minus model value transformed at the observation location and time). Together with the time series, the average value of weekly RMSs is evaluated over the qualification testing period (2019). The statistics are defined for all the Mediterranean Sea and are evaluated for the different assimilated satellites.

Name	Description	Ocean parameter	Supporting reference dataset	Quantity
NRT evaluation of Med-MFC-Currents using semi-independent data. Depth-Time Monthly comparison of misfits (Hovmoller diagrams)				
T-<X-Y>m-M-CLASS4–PROF-RMSD-MED-Jan2019-Dec2019-HOV	Temperature depth-time comparison with assimilated CMEMS INSITU TAC between 0 and 900m.	Temperature	Argo floats and XBT from the CMEMS INSITU TAC products: INSITU_MED_NRT_OBSERVATIONS_013_035	Depth-Time (Hovmoller diagram) of monthly RMS temperature misfits (observation minus model value transformed at the observation location and time) evaluated over the qualification testing period (2019). The statistics are averaged over the whole Mediterranean Sea and are defined between 0 and 900m depth.
S-<X-Y>m-M-CLASS4–PROF-RMSD-MED-Jan2019-Dec2019-HOV	Salinity depth-time comparison with assimilated CMEMS INSITU TAC between 0 and 900m.	Salinity	Argo floats from the CMEMS INSITU TAC products: INSITU_MED_NRT_OBSERVATIONS_013_035	Depth-Time (Hovmoller diagram) of monthly RMS salinity misfits (observation minus model value transformed at the observation location and time) evaluated over the qualification testing period (2019). The statistics are averaged over the whole Mediterranean Sea and are defined between 0 and 900m depth.
Name	**Description**	**Ocean parameter**	**Supporting reference dataset**	**Quantity**
NRT evaluation of Med-MFC-Currents using semi-independent data. 2D MAPS of Yearly comparison of misfits				
T-<X-Y>m-Y-CLASS4–PROF-RMSD-MED-Jan2019-Dec2019-2DMAP	Temperature comparison with assimilated CMEMS INSITU TAC data at 5 specified depths.	Temperature	Argo floats and XBT from the CMEMS INSITU TAC products: INSITU_MED_NRT_OBSERVATIONS_013_035	2D MAPS of RMS temperature misfits (observation minus model value transformed at the observation location and time) averaged over the qualification testing period (2019). The statistics are defined for all the Mediterranean Sea and are evaluated at five different depths: 8, 30, 150, 300 and 600 m.
S-<X-Y>m-Y-CLASS4–PROF-RMSD-MED-Jan2019-Dec2019-2DMAP	Salinity comparison with assimilated CMEMS INSITU TAC data at 5 specified depths.	Salinity	Argo floats from the CMEMS INSITU TAC products: INSITU_MED_NRT_OBSERVATIONS_013_035	2D MAPS of RMS salinity misfits (observation minus model value transformed at the observation location and time) averaged over the qualification testing period (2019). The statistics are defined for all the Mediterranean Sea and are evaluated at five different depths: 8, 30, 150, 300 and 600 m.
SLA-SURF-CLASS4–PROF-RMSD-MED-Jan2019-Dec2019-2DMAP	Sea Level Anomaly comparison with assimilated CMEMS INSITU TAC.	Sea Level	Satellites (Jason2, Jason2N, Jason3, CryoSat-2, Saral/Altika, S3A) Sea Level along track data: SEALEVEL_EUR_PHY_L3_REP_OBSERVATIONS_008_061 SEALEVEL_EUR_PHY_L3_NRT_OBSERVATIONS_008_059	2D MAPS of RMS Sea Level Anomaly misfits (observation minus model value transformed at the observation location and time) averaged over the qualification testing period (2019). The statistics are defined for all the Mediterranean Sea

Name	Description	Ocean parameter	Supporting reference dataset	Quantity
NRT evaluation of Med-MFC-Currents using independent data. Daily comparison with moorings				
UV-SURF-D-CLASS2-MOOR-RMSD-Jan2019-Dec2019	Surface currents comparison with CMEMS INSITU TAC	Currents	Moored buoys from CMEMS InSitu TAC products: INSITU_MED_NRT_OBSERVATIONS_013_035	Time series of daily sea surface currents of insitu observations and model outputs evaluated over the qualification testing period. Together with the time series, the average value of daily RMSs is evaluated over the qualification testing period. This quantity is evaluated on the model analysis.
UV-SURF-D-CLASS2-MOOR-BIAS-Jan2019-Dec2019	Surface currents comparison with CMEMS INSITU TAC	Currents	Moored buoys from CMEMS InSitu TAC products: INSITU_MED_NRT_OBSERVATIONS_013_035	Time series of daily sea surface currents of insitu observations and model outputs evaluated over the qualification testing period. Together with the time series, the average value of daily bias is evaluated over the qualification testing period. This quantity is evaluated on the model analysis.
Name	**Description**	**Ocean parameter**	**Supporting reference dataset**	**Quantity**
NRT evaluation of Med-MFC-Currents using Climatological dataset				
MLD-D-CLASS1-CLIM-MEAN_M-MED	Mixed Layer Depth comparison with climatology from literature in the Mediterranean Sea	Mixed Layer Depth	Monthly climatology from literature (Houpert et al., 2015)	Comparison of climatological maps form model outputs and a climatological dataset (Houpert at al., 2015)
SBT-D-CLASS4-CLIM-MEAN_M-MED	Bottom Temperature comparison with a climatological dataset in the Mediterranean Sea	Sea Bottom Temperature	SeaDataNet climatological datasets	Time series of monthly mean Sea Bottom Temperature from model outputs and SeaDataNetEAS4 climatologies. The time series are presented for the entire basin, for the area with topography < 500m and for the areas with topography < 1500m
SBT-D-CLASS1-CLIM-MEAN_M-MED	Bottom Temperature comparison with a climatological dataset in the Mediterranean Sea	Sea Bottom Temperature	SeaDataNet climatological datasets	Comparison of climatological maps form model outputs and SeaDataNet climatologies for the area with topography < 1500m

Table 7: (continued) List of metrics for Med-Currents evaluation using in-situ and satellite observations.

VALIDATION RESULTS

III.1 Temperature

In the following table are synthesised the values of the temperature Root Mean Square (RMS) of differences and bias calculated comparing the analysis of MEDSEA_ANALYSISFORECAST_PHY_006_013 product with quasi-independent data assimilated by the system (ARGO and Satellite SST). The synthesis is based on 1 year period (2019) validation and provided at 5 depths (8, 30, 150, 300, 600 m) showing that the larger error is achieved at 30 m depth while below it is lower than 0.3°C.

Variables/estimated accuracy:	Metrics		Depth (m)	Observation
SEA SURFACE TEMPERATURE (°C)	**RMS Diff**	**BIAS**		
	0.57±0.11	0.14±0.09	0	Satellite SST
TEMPERATURE (°C)	**RMS Diff**		**Depth (m)**	**Observation**
	0.58±0.22		8	Argo
	0.8±0.43		30	Argo
	0.28±0.05		150	Argo
	0.21±0.04		300	Argo
	0.11±0.02		600	Argo

Table 7: Quasi-independent validation. Analysis evaluation based over year 2019.

Figure 3 shows the time series of weekly RMS of temperature misfits at 5 depths (8, 30, 150, 300, 600 m), T-<X-Y>m-W-CLASS4–PROF-RMSD-MED-Jan2019-Dec2019, for the CMEMS Med-MFC-currents EAS6 system; the values of the mean RMS difference are reported in the legend of the figures; the number of observed profiles is represented in shaded coloured areas.

The temperature error is generally higher at depth around 30 m and has a better skill below 150 m. It presents a seasonal variability at first layers with higher values during warm seasons.

Monthly mean RMS of temperature misfits are represented in the following (Depth-Time) Hovmoller diagrams (Figure 4) along the water column between surface and 900 m showing the vertical pattern of the error averaged in the whole Mediterranean Sea. The system presents higher errors during summer-autumn seasons in the thermocline, between 30-60 m depth.

In addition to basin averaged statistics, the following panels in Figure 5 show the spatial pattern of the temperature RMSD averaged over the entire qualification period (2019) for the entire domain (top left panel) and at several layers (0-10, 10-100, 100-500, 500-1500 m) with respect to ARGO data. The top right panel shows the number of observations along the whole water column used for this analysis. The maps confirm that the largest discrepancy occurs between 10-100m. The largest differences are located in the eastern and western basins.
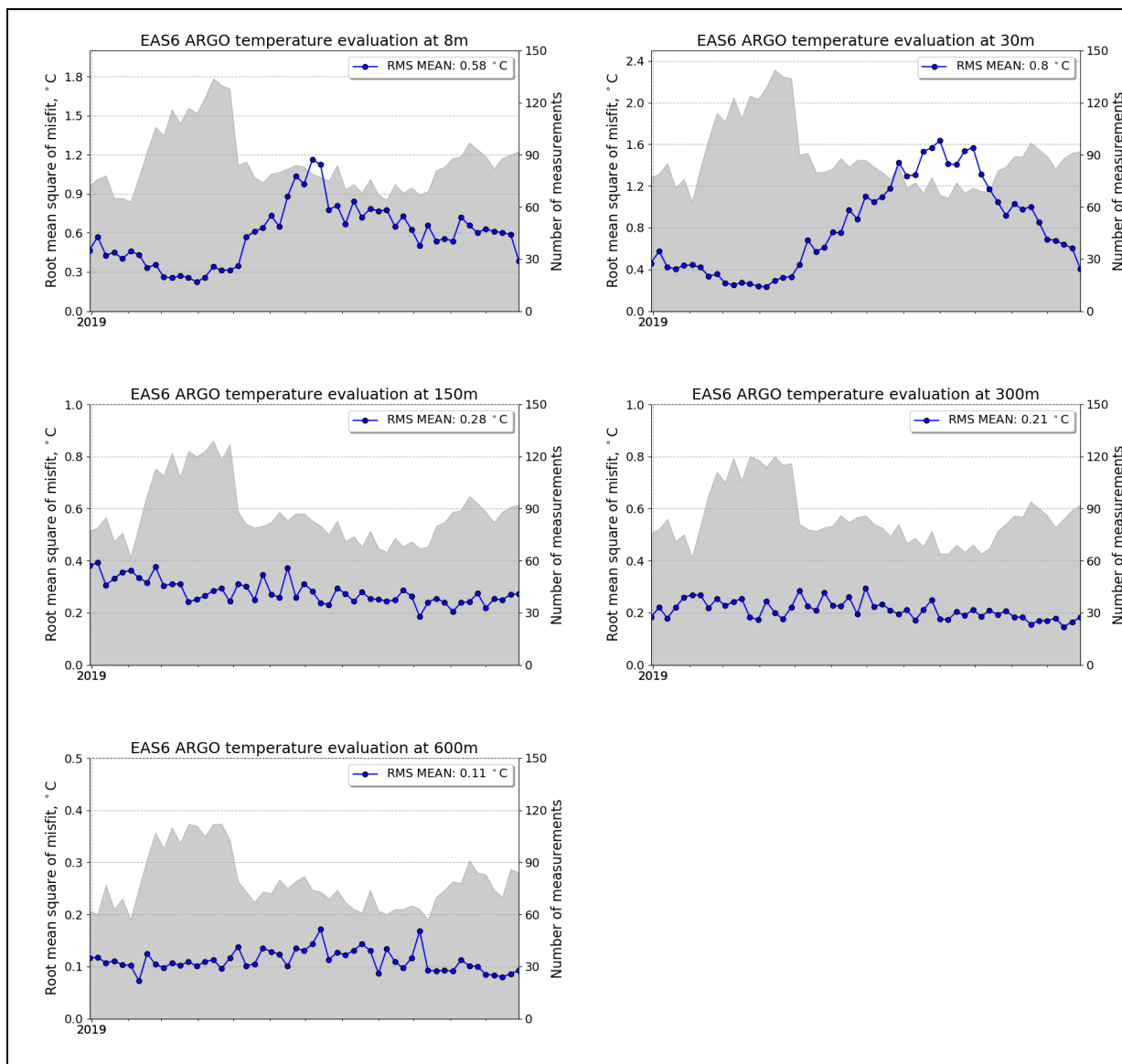
Figure 3: Time series of weekly RMS of temperature misfits (solid line) and number of observed profiles (shaded area) at 8, 30, 150, 300 and 600 m (T-<X-Y>m-W-CLASS4–PROF-RMS-MED-Jan2019-Dec 2019)
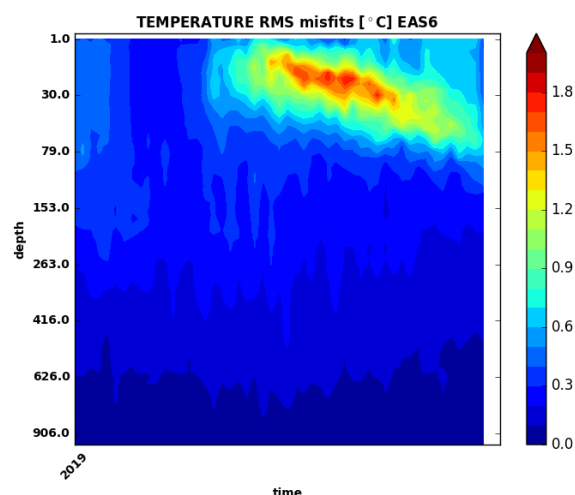
Figure 4: Hovmoller (Depth-Time) diagram of monthly mean RMS of temperature misfits along the water column averaged in the whole Mediterranean Sea during 2019 (T-<X-Y>m-M-CLASS4–PROF-RMSD-MED-Jan2019-Dec2019-HOV).
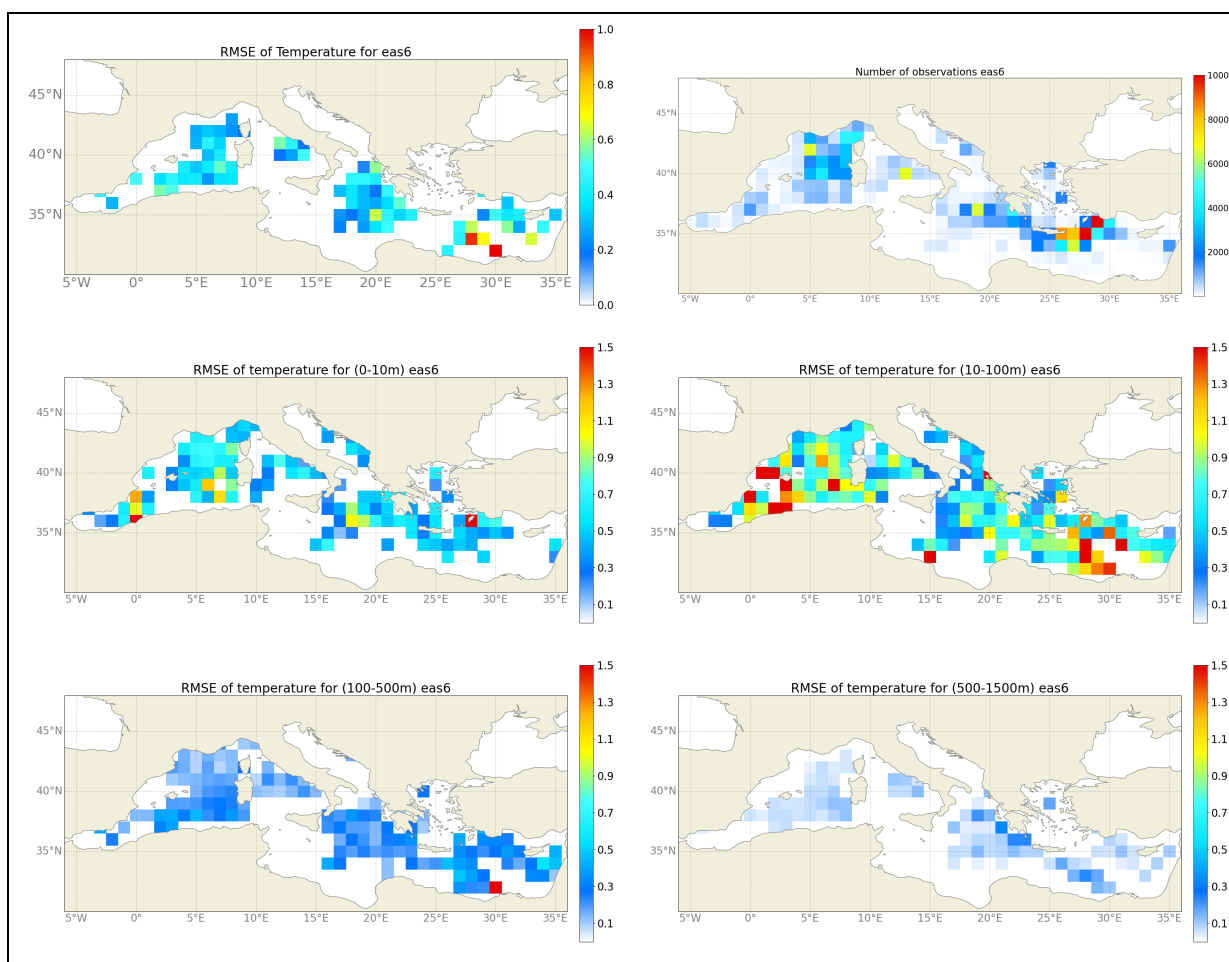

Figure 5: Maps of temperature RMSD averaged in the entire qualification period (2019). Top left: basin average RMSD; top right: n. of observations, middle left: RMSD averaged between 0-10 m; middle right: RMSD averaged between 10-100 m; bottom left: RMSD averaged between 100-500 m; bottom right RMSD averaged between 500-1500 m. (T-<X-Y>m-Y-CLASS4–PROF-RMSD-MED-Jan2019-Dec2019-2DMAP).

The following panels in Figure 6 show the time series of temperature daily RMS differences between model outputs and observations evaluated over the qualification period (2019) and indicate the number of observations used for this validation (grey bars). The statistics are evaluated for 4 different layers (0-10, 10-100, 100-500, 500-1500 m): T-<X-Y>m-D-CLASS4-RMSD-MED-Jan2019-Dec 2019. The average value of RMSD over the entire period is also reported in the figure.
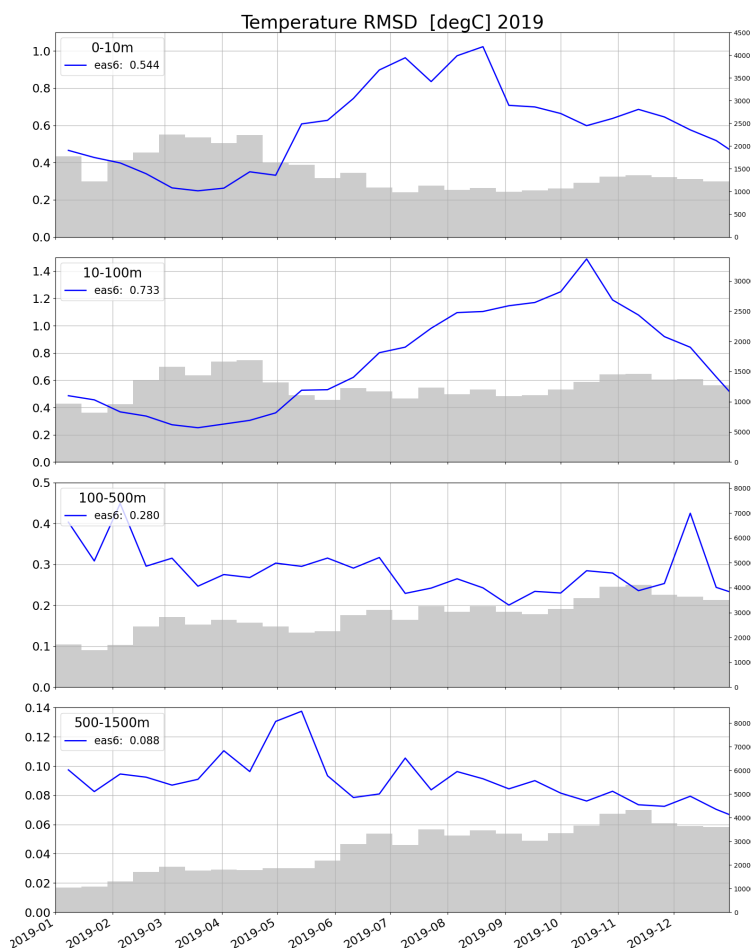
Figure 6: Time series of daily RMS of temperature at different vertical layers (T-<X-Y>m-D-CLASS4-RMSD-MED-Jan2019-Dec2019).

The temperature error is generally higher above 100 m and presents a clear seasonal variability with higher values during warm seasons, then the error decreases significantly below 100 m and at lower levels.

Figure 6 shows the time series of Sea Surface Temperature daily RMS difference (top) and BIAS (bottom) between daily model outputs and observations (L4 satellite SST at 1/16° resolution) evaluated over the qualification testing period (Jan-Dec 2019): SST-D-CLASS4-RAD-RMSD-Jan2019-Dec2019 and SST-D-CLASS4-RAD-BIAS-Jan2019-Dec2019.

The RMS of SST differences is higher during the warm season while it presents a minimum during spring. The SST bias is generally positive meaning that the model presents a warmer SST with respect to the observations. It has to be noted that here daily mean model outputs are compared to foundation SST (which is close to midnight SST).
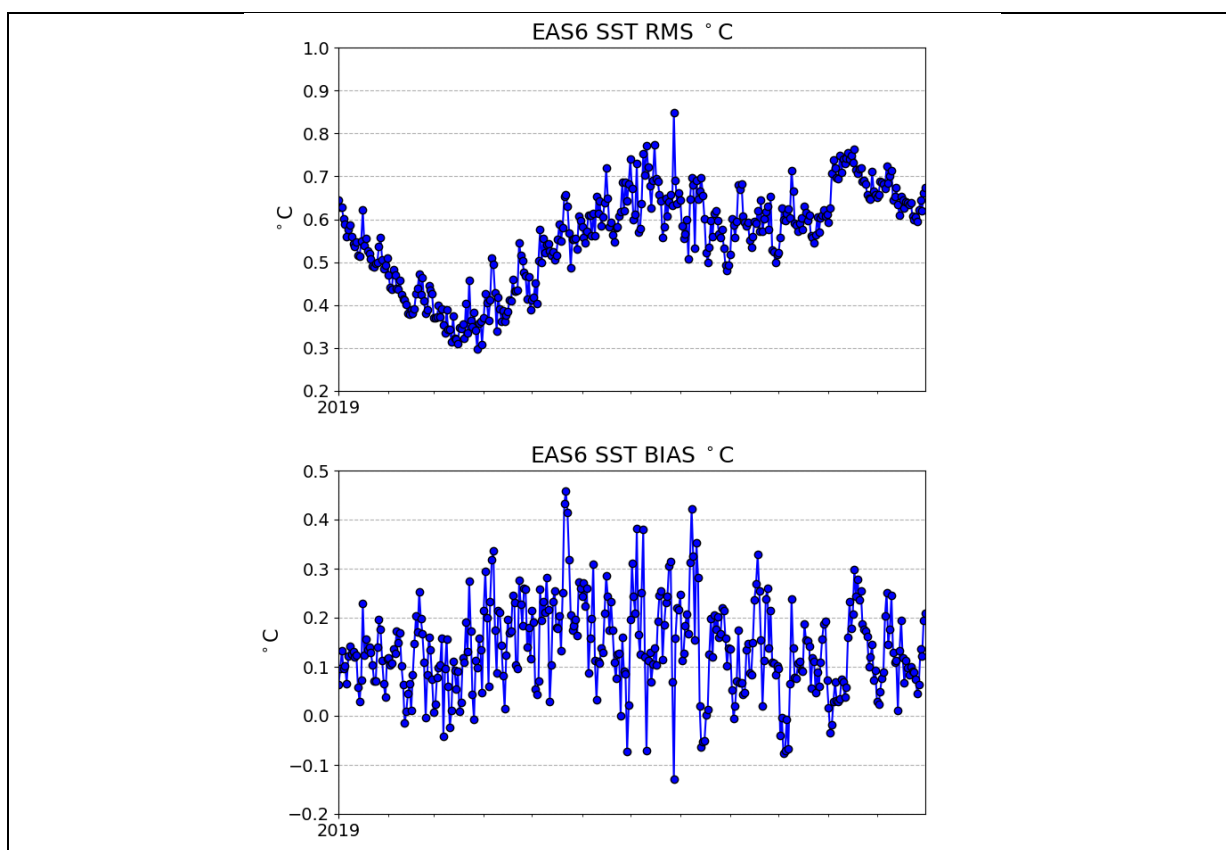
Figure 6: Time series of daily RMS difference (top) and Bias (bottom) of Sea Surface Temperature (SST-D-CLASS4-RAD-RMSD-Jan2019-Dec2019, SST-D-CLASS4-RAD-BIAS-Jan2019-Dec2019) with respect to satellite L4 data at 1/16° resolution.

III.2 Seabed Temperature

The bottom temperature, that is the temperature of the deepest level of the circulation model, has been compared to SeaDataNet climatology (see Tonani et al., 2013 for more details) for the year 2019.

Figure 7 shows the time series of the monthly climatological dataset (green line) and EAS6 system (blue line) evaluated as monthly averages for the year 2019. The left panel shows the climatological time series of seabed temperature at depths between [0-500] m, while the right panel shows the comparison at depths between [0-1500] m. The system is able to reproduce the seasonal variability of the bottom temperature that is generally overestimated by the model with respect to the climatological dataset.
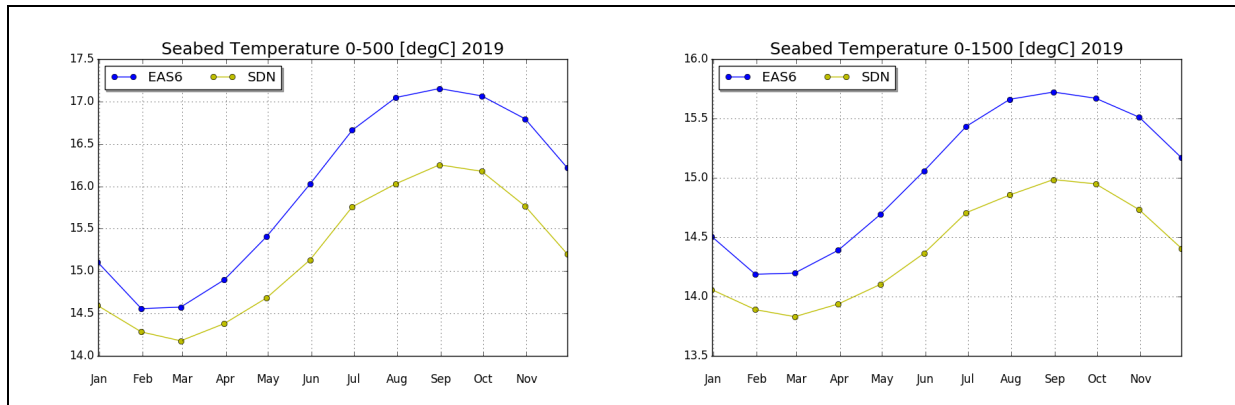
Figure 7: Time series of seabed temperature monthly climatology from SeaDataNet dataset (green line) and EAS6 system (blue line): SBT-D-CLASS4-CLIM-MEAN_M-MED.

The following figures show the January (Figure 8), April (Figure 9), July (Figure 10) and October (Figure 11) monthly mean seabed temperature in areas with topography included between 0 and 1500 m from SDN dataset (top), and corresponding monthly averages for Med-Currents EAS6 system (bottom) evaluated for the year 2019. The system exhibits similar temporal and spatial patterns compared to the climatological datasets. The main differences are related to warmer seabed temperature along several coastal areas predicted by the models with respect to the climatological dataset.
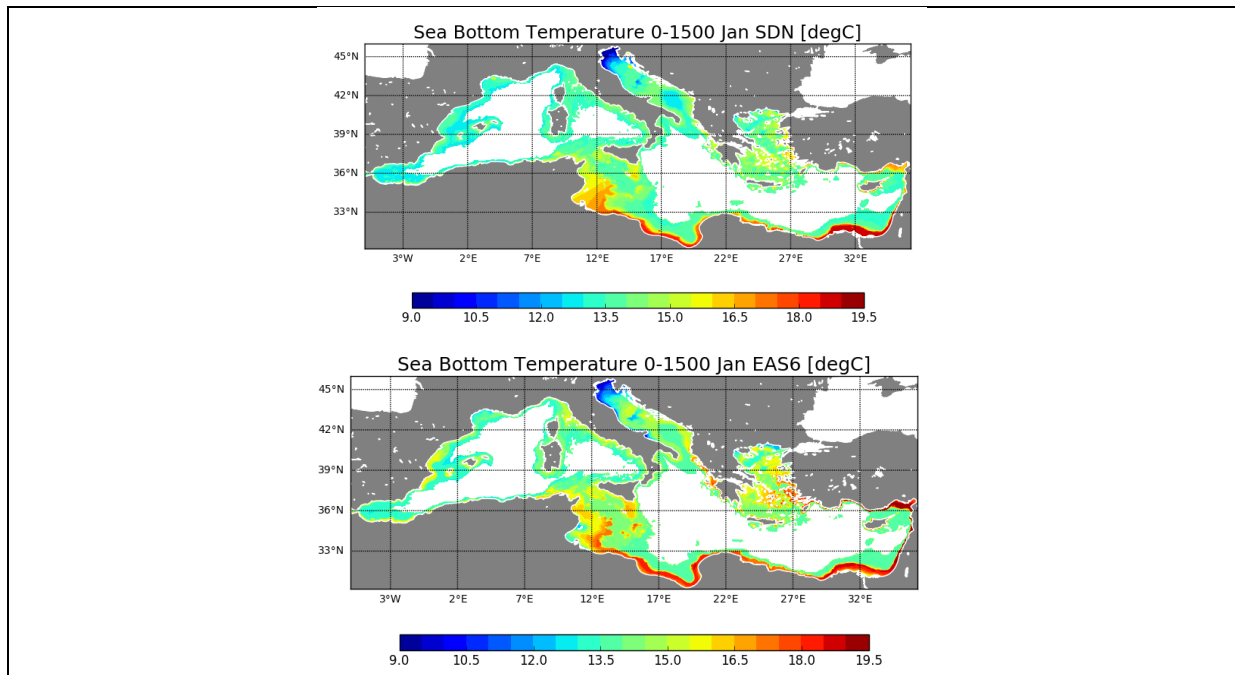
Figure 8: January Seabed temperature 2D maps in areas with topography lower than 1500 m: SDN climatology (top), monthly average Med-Currents EAS6 system (bottom): SBT-D-CLASS1-CLIM-MEAN_M-MED.
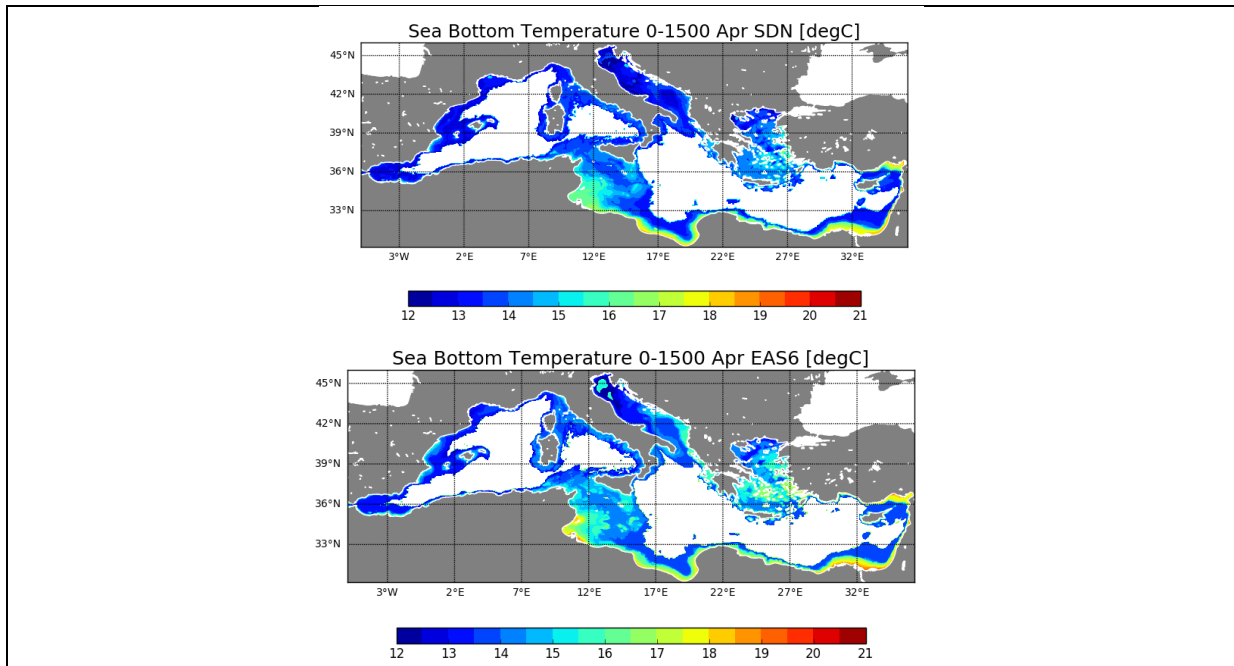
Figure 9: April Seabed temperature 2D maps in areas with topography lower than 1500 m: SDN climatology (top), monthly average Med-Currents EAS6 system (bottom): SBT-D-CLASS1-CLIM-MEAN_M-MED.
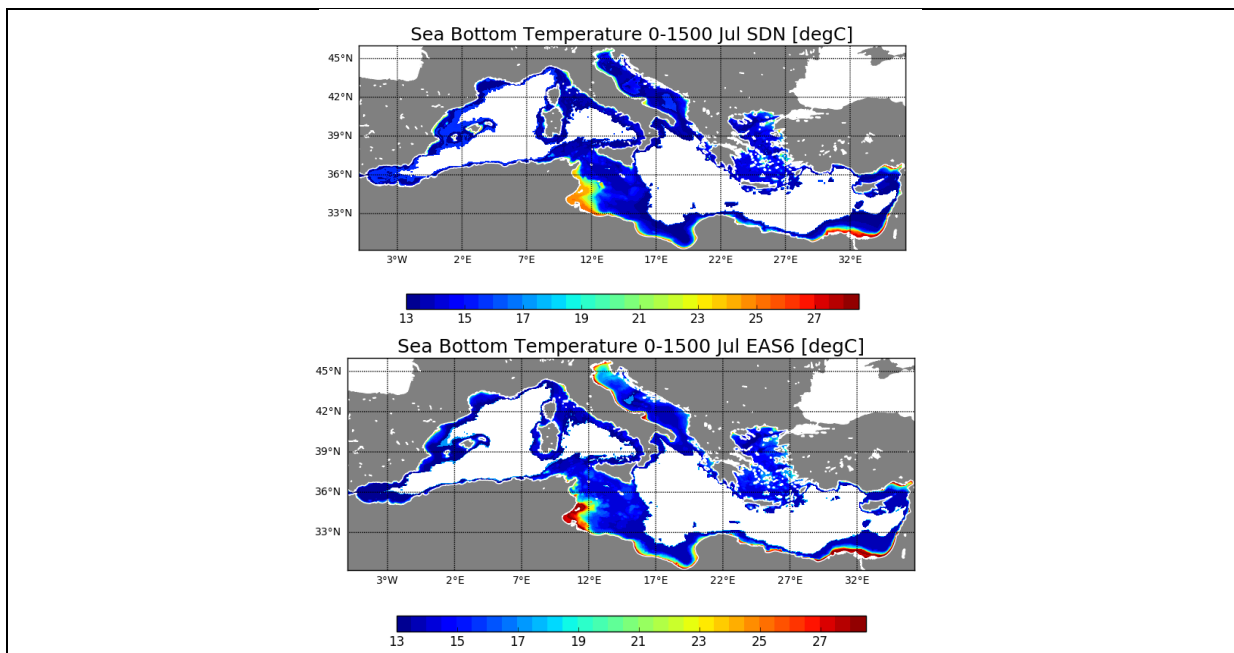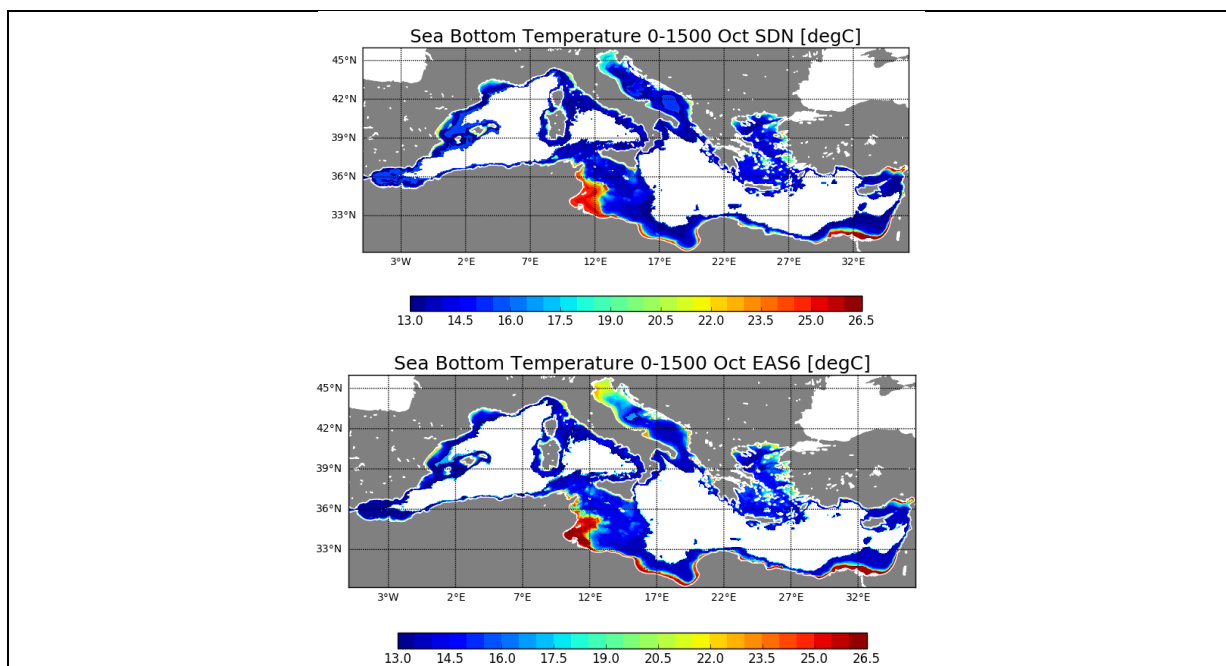

Figure 10: July Seabed temperature 2D maps in areas with topography lower than 1500 m: SDN climatology (top), monthly average Med-Currents EAS6 system (bottom): SBT-D-CLASS1-CLIM-MEAN_M-MED.

Figure 11: October Seabed temperature 2D maps in areas with topography lower than 1500 m: SDN climatology (top), monthly average Med-Currents EAS6 system (bottom): SBT-D-CLASS1-CLIM-MEAN_M-MED.

III.3 Salinity

In the following Table 8 there is a synthesis of the values of the salinity Root Mean Square (RMS) differences calculated comparing the analysis of MEDSEA_ANALYSISFORECAST_PHY_006_013 product with quasi-independent data assimilated by the system for salinity (ARGO).

The synthesis is based on 1 year period (2019) and provided at 5 depths (8, 30, 150, 300, 600 m). The error is always lower than 0.15 PSU and it is higher at surface and decreases significantly below 150 m.

Variables/estimated accuracy:	Metrics	Depth	Observation
	RMS Diff	[m]	Instrument
SALINITY (PSU)	0.15±0.03	8	Argo
	0.16±0.04	30	Argo
	0.1±0.02	150	Argo
	0.05±0.01	300	Argo
	0.03±0	600	Argo

Table 8: Quasi-independent validation. Analysis evaluation based over year 2019.

The panels in Figure 12 show the time series of weekly RMS of salinity misfits (observation minus model value transformed at the observation location and time before being assimilated) at 5 depths (8, 30, 150, 300, 600 m), S-<X-Y>m-W-CLASS4–PROF-RMSD-MED-Jan2019-Dec2019; the values of the mean RMS differences are reported in the legend of the figures; the number of observed profiles that have been assimilated are represented as shaded areas.

The salinity error is generally higher above 30 m with values less than 0.16 PSU and better skill below 150 m with values lower than 0.1 PSU.
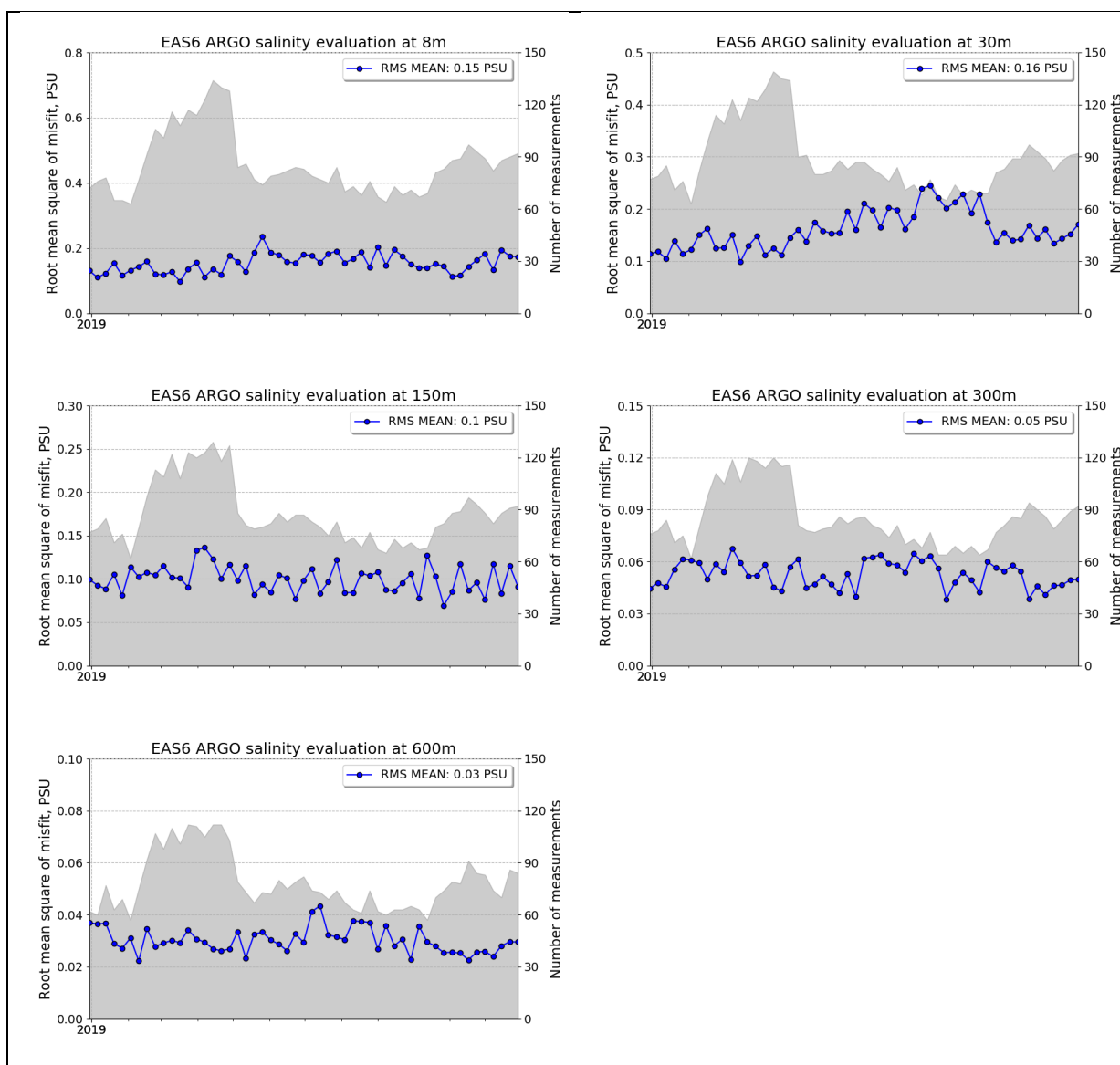
Figure 12: Time series of weekly RMS of salinity misfits ARGO-Model (solid lines) and number of observed profiles (shaded area) at 8, 30, 150, 300 and 600 m (S-<X-Y>m-W-CLASS4–PROF-RMSD-MED-Jan2019-Dec2019).

Monthly mean RMS of salinity misfits are represented in the following Figure 13 by means of Hovmoller diagrams (Depth-Time) along the water column between surface and 900 m depth showing the vertical pattern of the error averaged in the whole Mediterranean Sea. The system presents higher errors in the upper layers decreasing below 150 m.
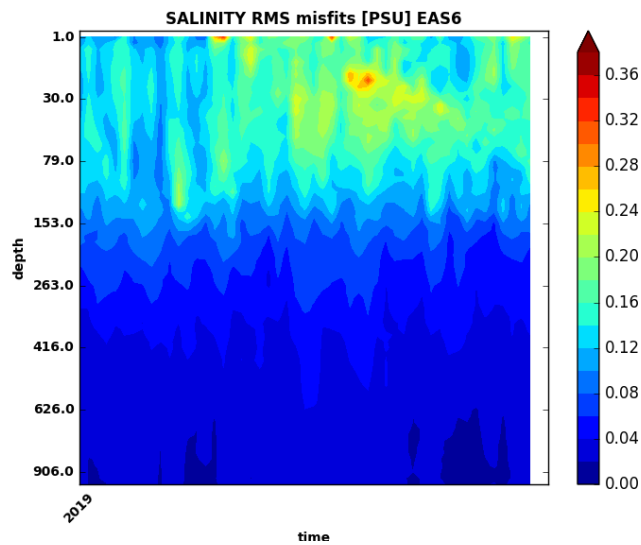
Figure 13: Hovmoller (Depth-Time) diagram of monthly mean RMS of salinity misfits along the water column averaged in the whole Mediterranean Sea (S-<X-Y>m-M-CLASS4–PROF-RMSD-MED-Jan2019-Dec2019-HOV).

In addition to basin averaged statistics, the following panels in Figure 14 show the spatial pattern of the salinity RMSD averaged over the entire qualification period (2019) for the entire domain (top left panel) and at several layers (0-10, 10-100, 100-500, 500-1500 m) with respect to ARGO data. The top right panel shows the number of observations along the whole water column used for this analysis. The maps confirm that the largest discrepancy appears between 10-100 m. The largest differences are located in the eastern and western basin.
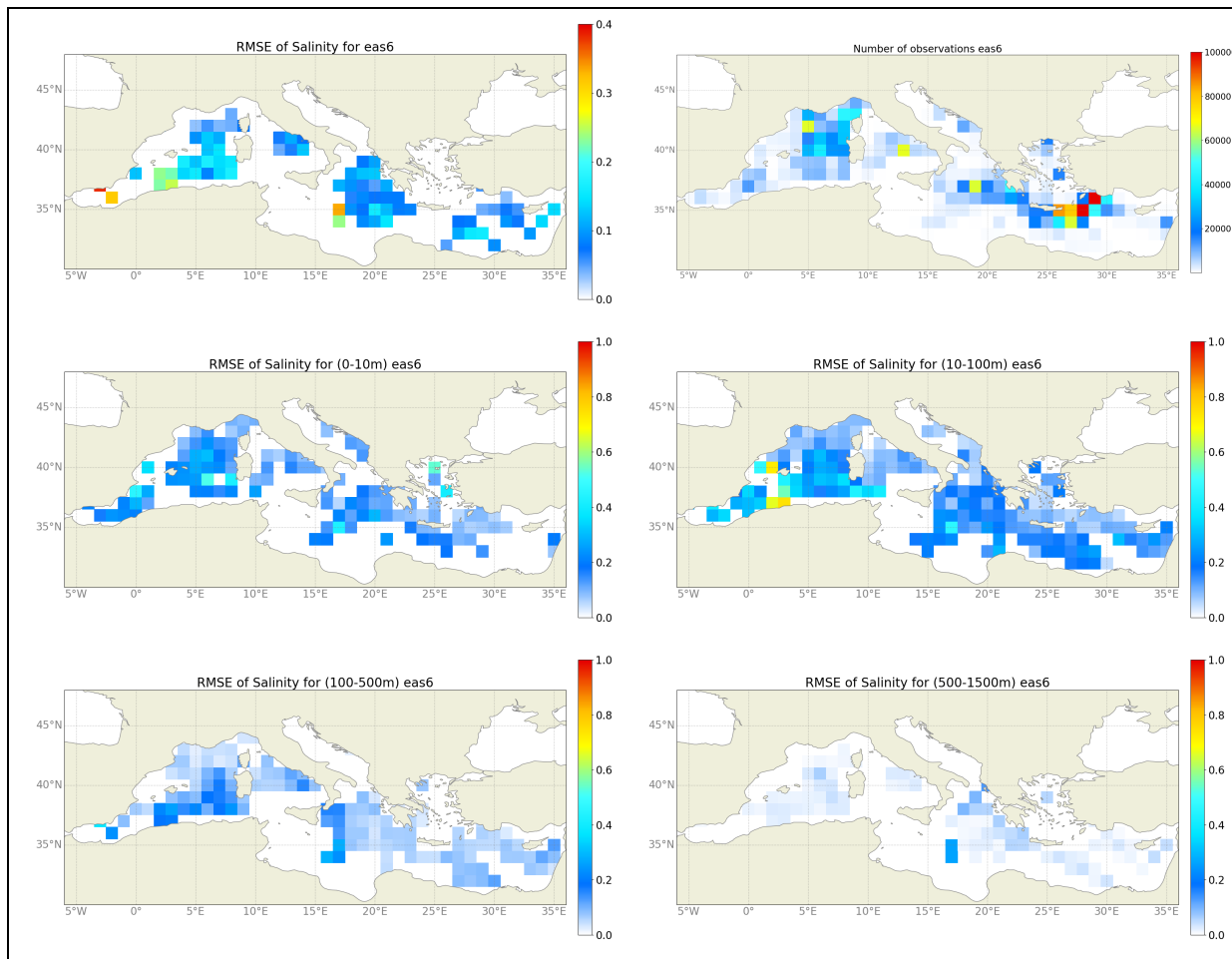
Figure 14: Maps of salinity RMSD averaged in the entire qualification period (2019). Top left: basin average RMSD; top right: n. of observations, middle left: RMSD averaged between 0-10m; middle right: RMSD averaged between 10-100m; bottom left: RMSD averaged between 100-500 m; bottom right RMSD averaged between 500-1500 m. (S-<X-Y>m-Y-CLASS4–PROF-RMSD-MED-Jan2019-Dec2019-2DMAP).

The following panels in Figure 15 show the time series of salinity daily RMSs of the difference between model outputs and observations evaluated over the qualification testing period (2019): S-<X-Y>m-D-CLASS4-PROF-RMSD-MED-Jan2019-Dec2019. The statistics are evaluated for four different layers (0-10, 10-100, 100-500, 500-1500 m). The average value of RMS difference over the entire period is presented in the figure. The salinity error is generally higher above 150 m then the error decreases significantly below 150 m.

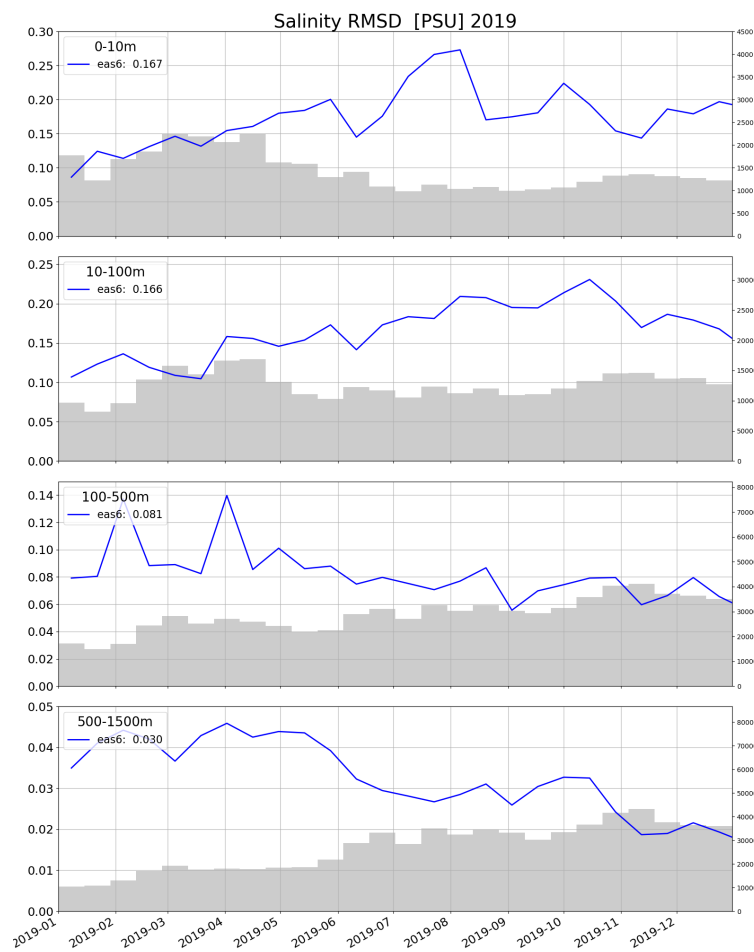COPERNICUS MARINE ENVIRONMENT MONITORING SERVICE

Figure 15: Time series of daily RMSD of salinity at different vertical layers (S-<X-Y>m-D-CLASS4-PROF-RMSD-MED-Jan2019-Dec2019).

III.4 Sea Level

In Table 10 there are the RMS differences for the Sea Level Anomaly calculated comparing the analysis of MEDSEA_ANALYSISFORECAST_PHY_006_013 product with each available satellite (along track observations) from January to December 2019.

SEA LEVEL ANOMALIES	RMS Diff (cm)	Availability
All Satellites	3.4	01/01/2019-13/05/2019
ALTIKA	3.3	01/01/2019-13/05/2019
CRYOSAT	3.4	01/01/2019-31/12/2019
JASON 2G	3.4	22/05/2019-25/09/2019
JASON3	3.4	01/01/2019-31/12/2019
SENTINEL3A	3.3	01/01/2019-31/12/2019
SENTINEL3B	3.4	01/01/2019-31/12/2019
SENTINEL6A	2.9	28 March - 28 June 2022

Table 9: Analysis evaluation based over 1 year time series (2019) for the Sea Level Anomaly for each available satellite.

The following Figure 16 shows the time series of weekly RMS of sea level anomaly misfits (observation minus model value transformed at the observation location and time before being assimilated), SLA-SURF-W-CLASS4-ALT-RMSD-MED-Jan2019-Dec2019, the number of assimilated data is provided as shaded areas.

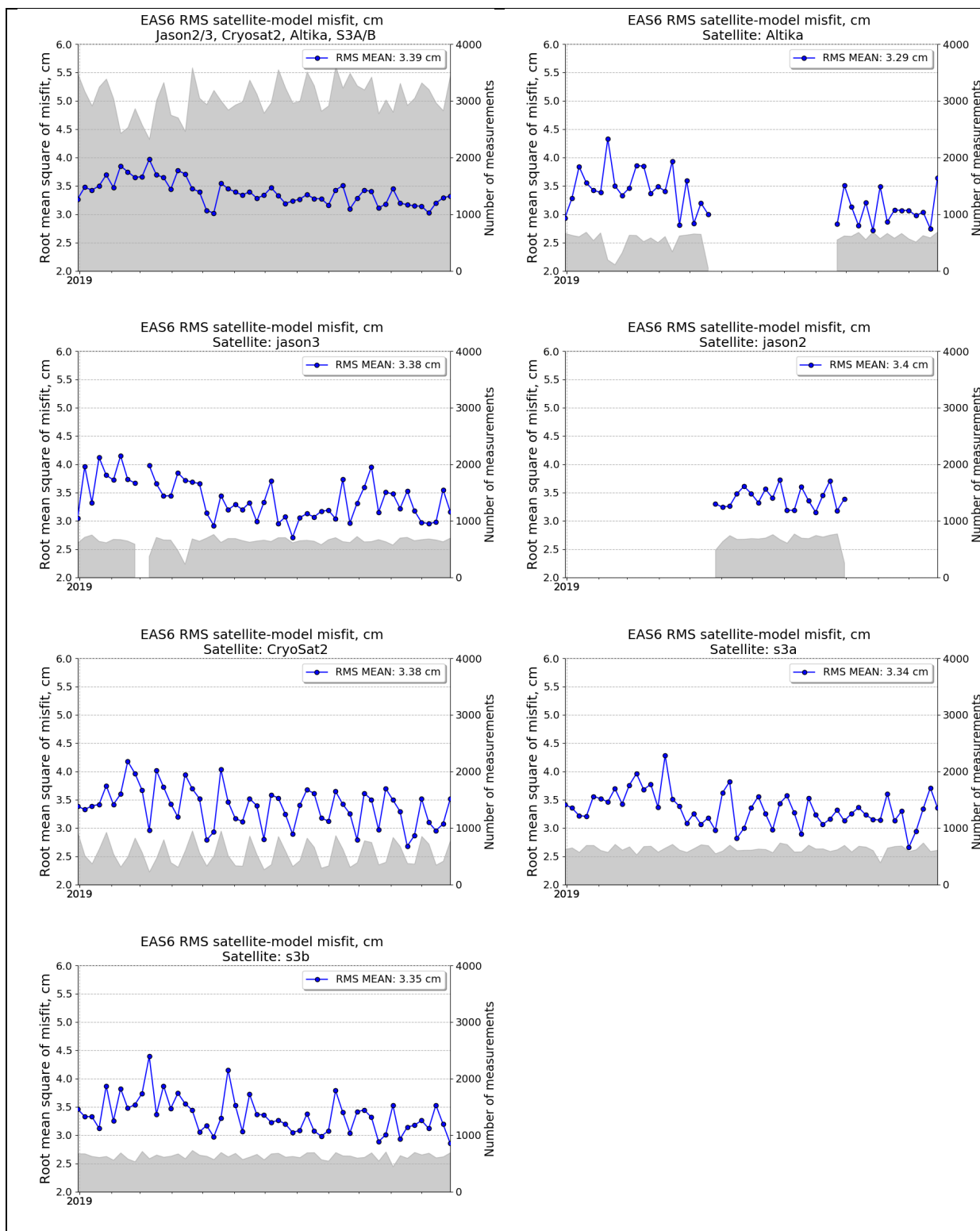The system an overall error of about 3.4 cm in the whole basin.

Figure 16 Time series of weekly RMS of misfits along SLA data track for all the satellites, Altika, Cryosat, Jason2G, Jason3, Sentinel3A and Sentinel3B and corresponding number of assimilated data (shaded areas in the figures) (SLA-SURF-W-CLASS4-ALT-RMSD-MED-Jan2019-Dec2019).

In addition to basin averaged statistics, the following figures (Figure 17) show the spatial pattern of the Sea Level Anomaly RMS misfits (top panel) averaged in the entire qualification period (2019) with respect to SLA tracks and the number of data used for this analysis (bottom panel).
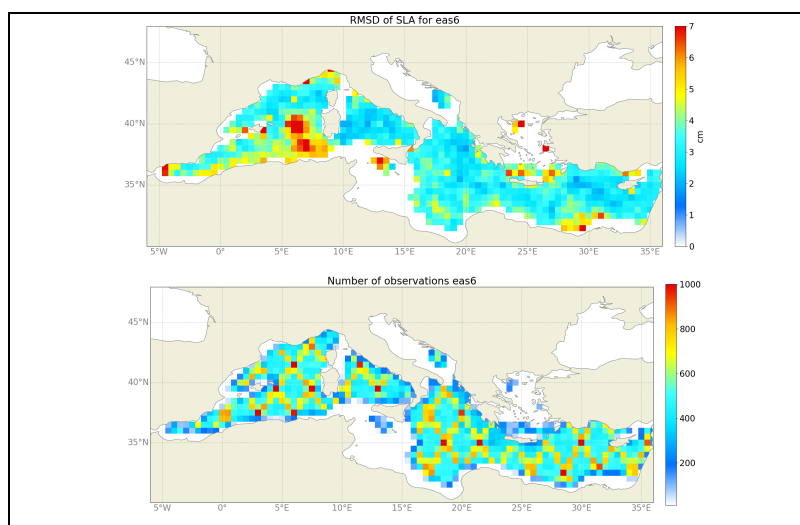
Figure 17: Maps of Sea Level Anomaly RMS misfits (top) averaged in the entire qualification period (2019) with respect to SLA L3 along track Altimetry data and number of data used for this analysis (bottom) (SLA-SURF-CLASS4–PROF-RMSD-MED-Jan2019-Dec2019-2DMAP).

Figure 18 shows the time series of the RMS of the sea level anomaly difference between daily model outputs and observations evaluated over the qualification testing period (2019), with an average RMSD value of 3.6 cm.
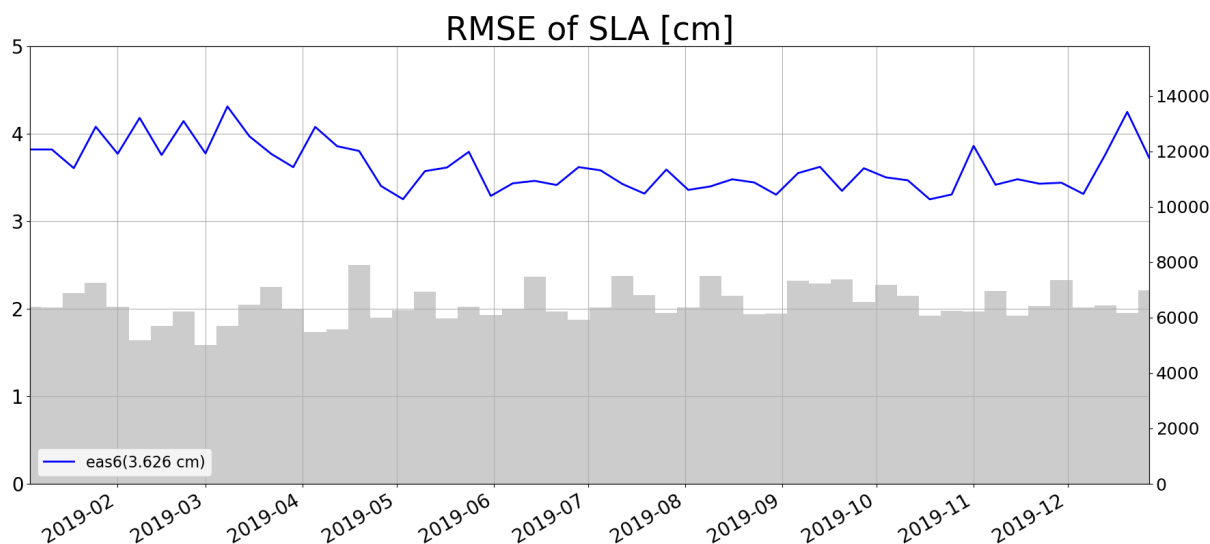

Figure 18: Time series of daily RMSD of Sea Level Anomaly (SLA-SURF-D-CLASS4-RMSD-MED-Jan2019-Dec 2019)

III.5 Currents

The predicted sea surface currents skill is assessed by means of independent validation through coastal moorings.

Table 10 summarizes the RMS differences and the bias calculated comparing the analysis of MEDSEA_ANALYSISFORECAST_PHY_006_013 product with the independent in-situ data (MB: coastal moored buoys) for the year 2019.

Variables/estimated accuracy:	RMS diff	Bias	Depth	Obs	No. of Obs.
	UV-SURF-D-CLASS2-MOOR-RMSD-Jan2019-Dec2019	UV-SURF-D-CLASS2-MOOR-BIAS-Jan2019-Dec2019			
Current (m/s) year 2019: EAS6	0.135	-0.056	0-3	MB	10

Table 10: Independent observation evaluation based on 1-year time series (2019) of analysis and Moored Buoys observations.

Figure 19 shows an example of daily sea surface currents time series of EAS6 (blue line) daily mean model outputs against the Cabo de Gata (n. 6100198) coastal mooring (green line) for year 2019, the figure presents also the bias and RMS difference.
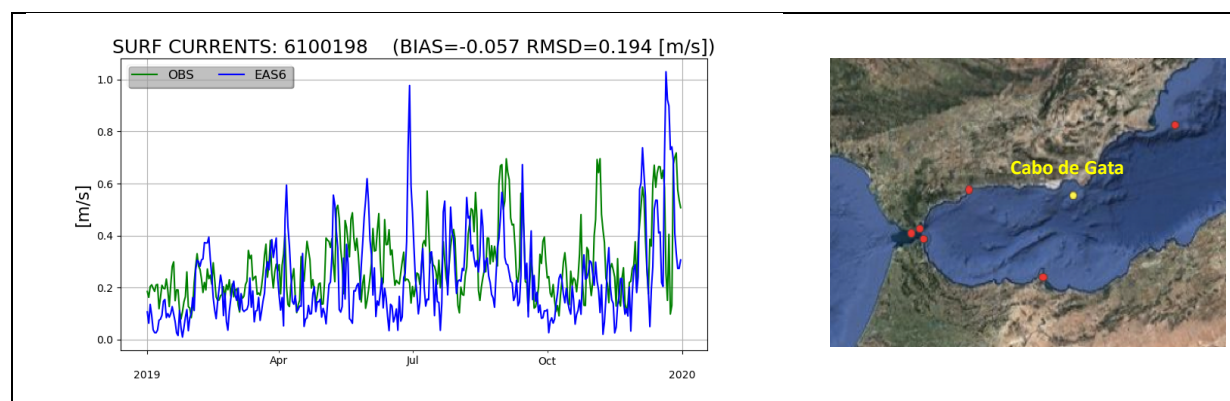

Figure 19: Left: Time series of daily sea surface currents at Cabo de Gata buoy. Comparison between observations (green line) and EAS5 model outputs (blue line). (UV-SURF-D-CLASS2-MOOR-RMSD-Jan2019-Dec2019, UV-SURF-D-CLASS2-MOOR-BIAS-Jan2019-Dec2019). Right: Cabo de Gata Buoy location.

In addition to surface current validation, an assessment of velocity derived variables is provided in terms of transport through the strait of Gibraltar.

In Figure 20 the time series of the mean daily net, eastward and westward fluxes through the Gibraltar Strait during 2019 are represented.
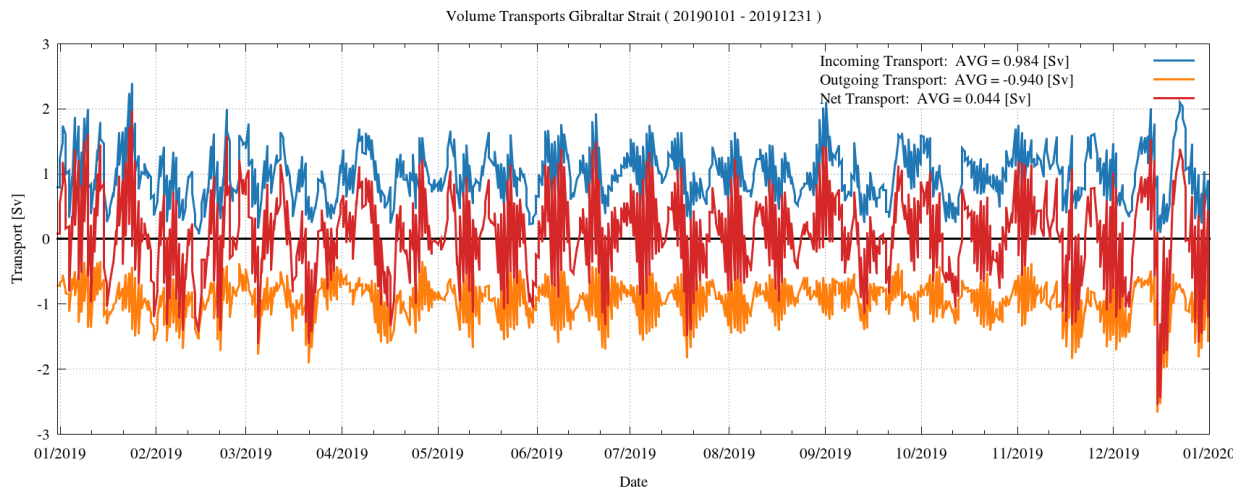
Figure 20: Time series of daily mean Net (red), Eastward (blue) and Westward (orange) fluxes through the Gibraltar Strait in 2019.

In Table 11 the comparison of the mean net, eastward and westward transports with respect to literature fluxes (Soto-Navaro et al., 2010) is included. In order to compare these values with literature, in addition to the 2019 annual mean transports, a longer period evaluation has been reported showing the 4 year mean (2016-2019) transports.

Gibraltar Mean Transport	EAS6 (2019)	EAS6 (2016-2019)	Soto-Navarro et al., 2010
Net	0.044 Sv	0.041	0.038 ± 0.007
Eastward	0.984 Sv	0.973	0.81 ± 0.06
Westward	0.940 Sv	0.932	0.78 ± 0.05

Table 11: Gibraltar mean fluxes [Sv] for EAS6 system averaged in the year 2019 and for a longer period (2016-2019) compared to literature values.

III.6 Mixed Layer Depth

In order to assess the model ability to reproduce the Mixed Layer Depth (MLD), monthly averaged 2D maps of MLD have been compared to a climatological dataset available from literature (Houpert et al., 2015) providing monthly gridded climatology produced using MBT, XBT, Profiling floats, Gliders, and ship-based CTD data from different database and carried out in the Mediterranean Sea between 1969 and 2013. Figure 21 to Figure 24 show the 2D maps of climatological MLD from literature (top), monthly averaged MLD from MED-Currents EAS6 system (bottom).

It can be noticed that during February 2019 (Figure 21), the deepening of the MLD in the Gulf of Lyon and in the South Adriatic areas are well represented by the model, which present for this year a deeper MLD in the Aegean See than the one shown in the climatological fields. During June and August 2019 (Figure 22 and Figure 23) the modelled MLD is in general very similar to the climatological one showing a low MLD. In December 2019 (Figure 24) the deepening of the MLD is well represented by the EAS6 system.

In general, it can be noticed that the EAS6 numerical system is able to represent the spatial and seasonal distribution of the MLD and the main differences can be due to the low resolution of the climatological dataset that moreover do not cover the whole domain of the Mediterranean Sea as well as on the different period of evaluation, being the Mediterranean Sea characterized by areas of deep-water formation whose deepening can significantly vary in time.
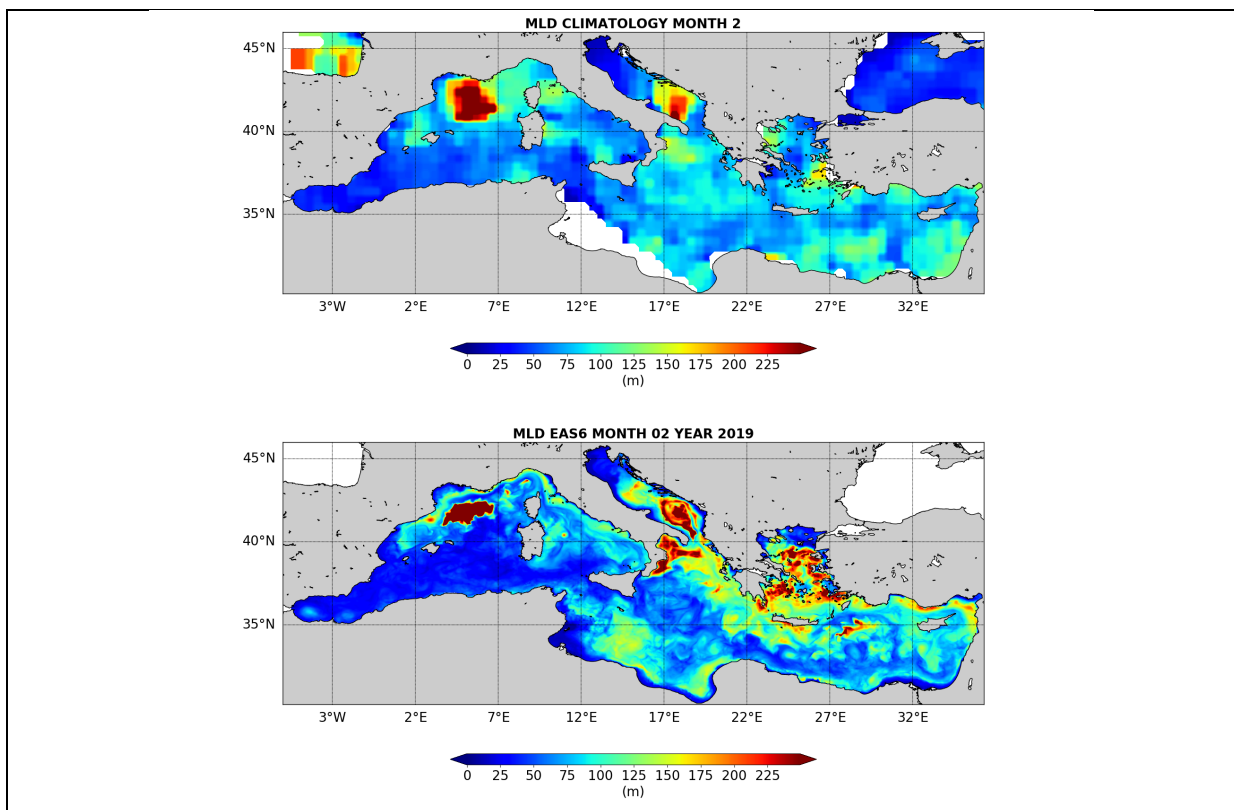

Figure 21: February MLD 2D maps. Top: climatological data from literature; bottom: February 2019 monthly averaged MLD from MED-Currents EAS6 system: MLD-D-CLASS1-CLIM-MEAN_M-MED
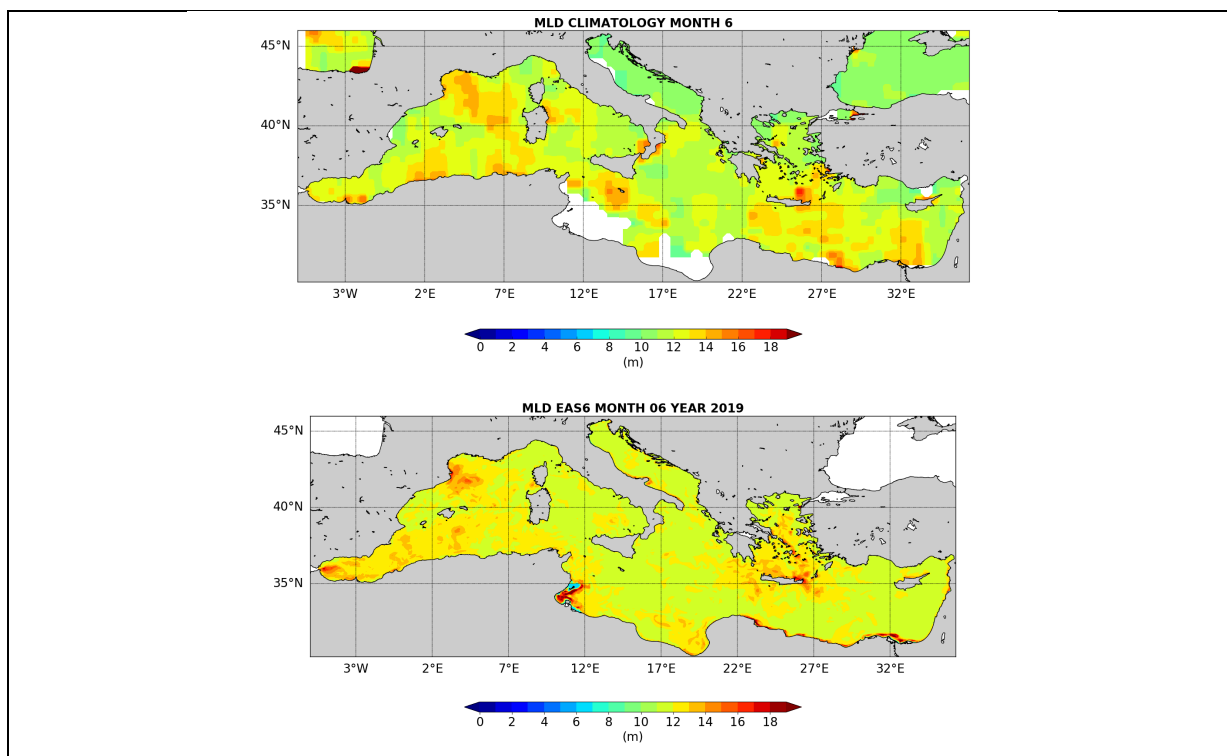
Figure 22: June MLD 2D maps. Top: climatological data from literature; bottom: June 2019 monthly averaged MLD from MED-Currents EAS6 system: MLD-D-CLASS1-CLIM-MEAN_M-MED
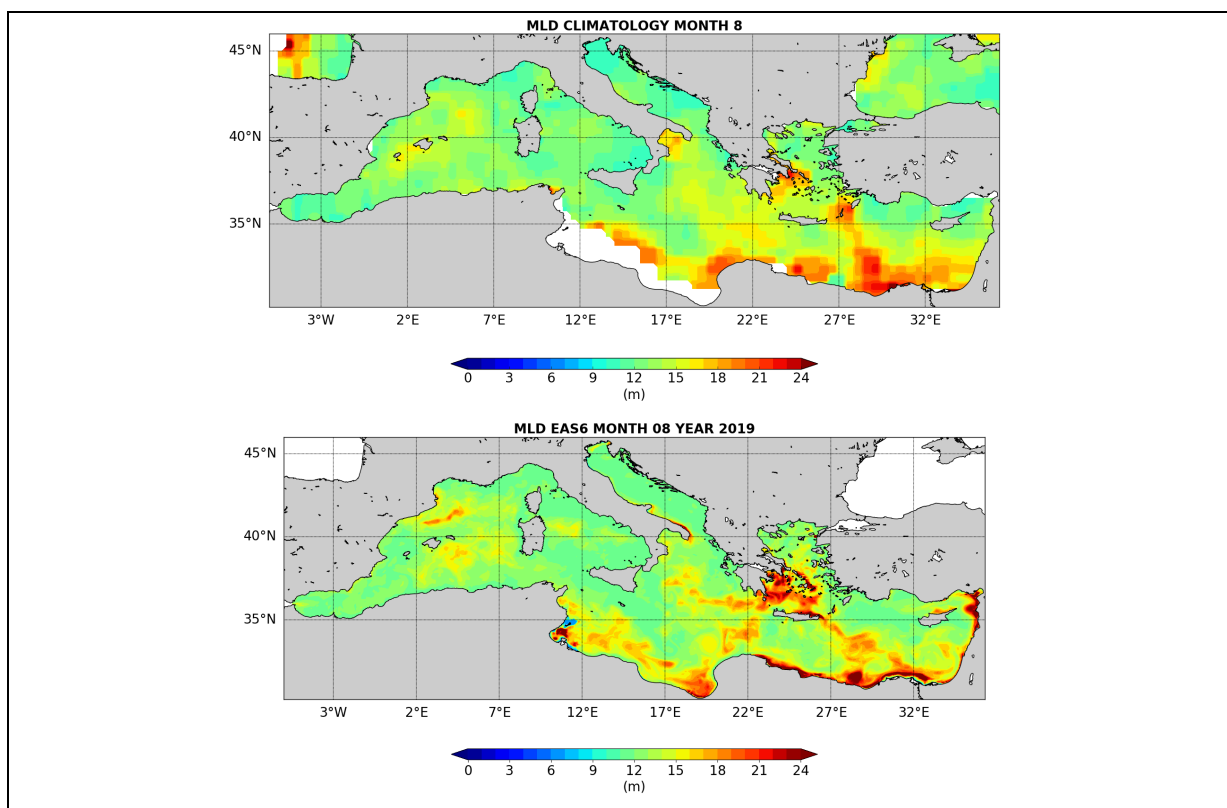

Figure 23: August MLD 2D maps. Top: climatological data from literature; bottom: August 2019 monthly averaged MLD from MED-Currents EAS6 system: MLD-D-CLASS1-CLIM-MEAN_M-MED
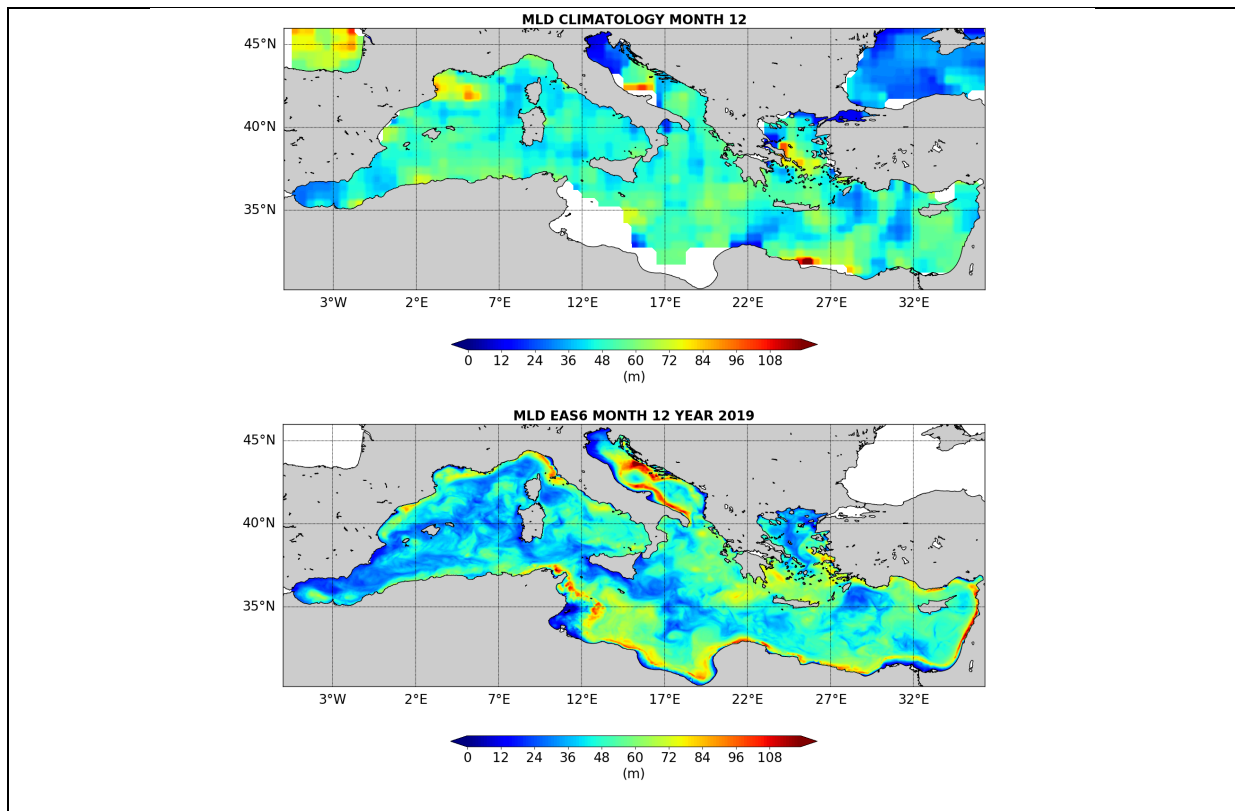
Figure 24: December MLD 2D maps. Top: climatological data from literature; bottom: December 2019 monthly averaged MLD from MED-Currents EAS6 system: MLD-D-CLASS1-CLIM-MEAN_M-MED

III.7 Harmonic Analysis

A specific analysis has been performed to evaluate the quality of EAS6 system including tides to verify its ability to reproduce the tidal amplitudes and phases of each tidal component. This is performed by means of an harmonic analysis based on 6 months period applied to the hourly sea level fields. Figure 25 shows the location of the tide gauges that have been used for this analysis, different colours represent different areas of the basin, while the numbers refer to the tide gauges listed in the following table.
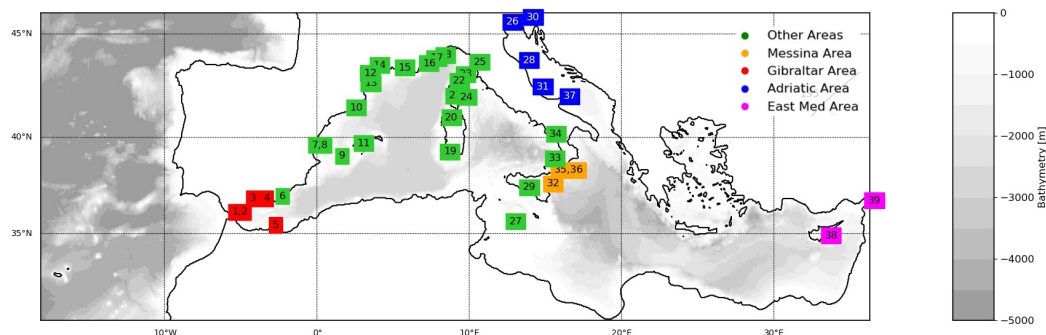

Figure 25: Location of the Mediterranean tide gauges used to perform the harmonic analysis

#	Name	Longitude	Latitude	Source
1	**Tarifa**	-5.60361	36.0064	EMODnet
2	Algeciras	-5.39833	36.1769	EMODnet
3	**Malaga**	-4.417	36.712	EMODnet
4	Motril	-3.524	36.72	EMODnet
5	Melilla	-2.918	35.291	EMODnet
6	**Almeria**	-2.478	36.83	EMODnet
7	Valencia	-0.33	39.46	EMODnet
8	Sagunto	-0.206	39.634	EMODnet
9	Ibiza	1.44972	38.9111	EMODnet
10	Barcelona	2.163	41.342	EMODnet
11	PalmadeMallorca	2.6375	39.5603	EMODnet
12	PortLaNouvelle	3.06410	43.01471	EMODnet
13	PortVendres	3.10730	42.52010	EMODnet
14	Sete	3.70170	43.40000	EMODnet
15	**Marseille**	5.35370	43.27850	EMODnet
16	LaFigueirette	6.93377	43.48353	EMODnet
17	Monaco	7.42370	43.73300	EMODnet
18	Imperia	8.01694	43.88111	ISPRA
19	**Carloforte**	8.30500	39.13556	ISPRA
20	Portotorres	8.40667	40.84722	ISPRA
21	Ajaccio	8.76290	41.92270	EMODnet
22	IleRousse	8.93524	42.63960	EMODnet
23	Centuri	9.34983	42.96578	EMODnet
24	Solenzara	9.40383	41.85686	EMODnet
25	**Livorno**	10.28806	43.54222	ISPRA
26	**Venezia**	12.42361	45.42361	ISPRA
27	**Lampedusa**	12.61000	35.49139	ISPRA
28	**Ancona**	13.50833	43.62694	ISPRA
29	**Porto Empedocle**	13.52528	37.28806	ISPRA
30	**Trieste**	13.76250	45.64389	ISPRA
31	**Ortona**	14.40667	42.35583	ISPRA
32	**Catania**	15.08472	37.49139	ISPRA
33	Ginostra	38.784	15.1933	EMODnet
34	Palinuro	15.27111	40.01694	ISPRA
35	Messina	15.55917	38.18639	ISPRA
36	**Reggio Calabria**	15.64389	38.11861	ISPRA
37	**Vieste**	16.16944	41.89806	ISPRA
38	Zygi	33.34023	34.72632	EMODnet
39	Iskenderun	36.17676	36.59423	EMODnet

Table 12: List of tide gauges used to perform the harmonic analysis: name, location and source

Figure 26 shows the amplitude and phase scatter plots for the 4 major tidal constituents: M2, S2, K1, O1: Model versus observations. This analysis shows a very good agreement between the model and observations.
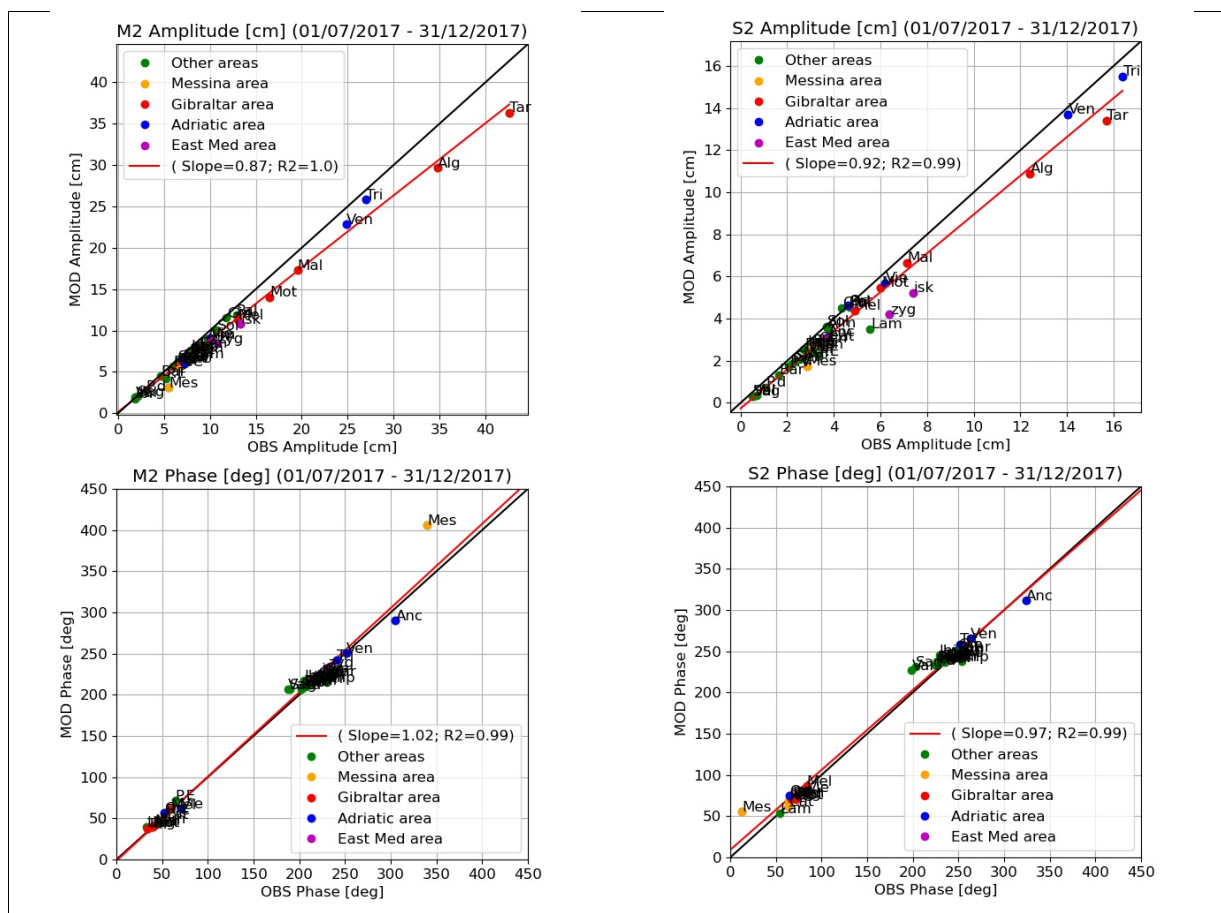

Figure 26: Scatter plot of tidal amplitude and phase for the 4 major Mediterranean Sea tidal constituents: M2, S2, K1, O1 evaluated at 39 tide gauges (continues in next page).
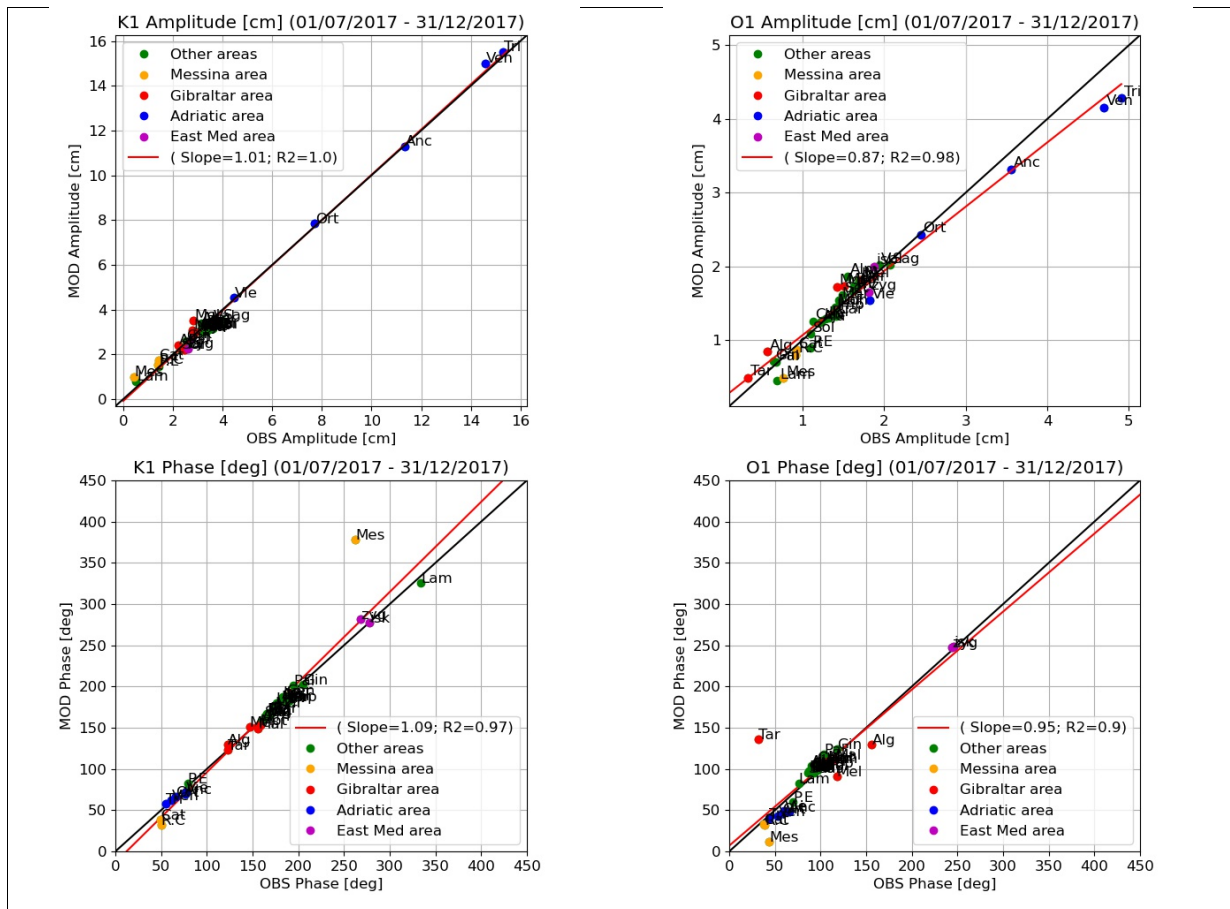
Figure 26: (continues) Scatter plot of tidal amplitude and phase for the 4 major Mediterranean Sea tidal constituents: M2, S2, K1, O1 evaluated at 39 tide gauges.

Figure 27 presents the RMSD evaluated from the tidal amplitude vectorial distance for each constituent, showing that the M2 component has the largest error, but it has to be considered that the amplitude of M2 tidal component is almost everywhere the greatest one.
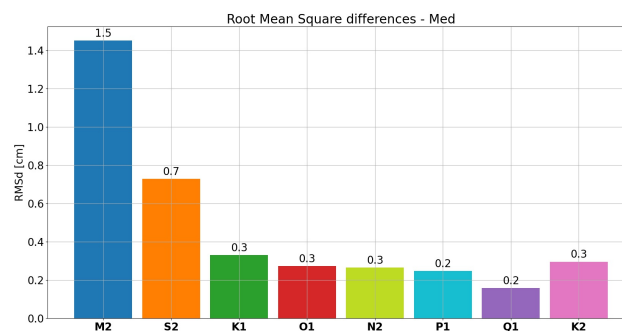

Figure 27. RMSD of vectorial distance between model and tide gauges tidal amplitudes for each tidal constituent

A further analysis has been performed by evaluating the vectorial distance between the model and a sub-set of tide gauges (#15) which were used in previous literature evaluations (Tsimplis et al. 1995, Palma et al. 2020). A table with the mean vectorial distances evaluated for EAS6 and the ones published

on reference literature is presented below, showing that EAS6 is almost always closer to observations with respect to previous studies.

Mean Vectorial distances	M2	S2	K1	O1
EAS56	1.78 cm	0.99 cm	0.44 cm	0.40 cm
Tsimplis et al., 1995	1.75 cm	1.21 cm	1.48 cm	0.46 cm
Palma et al., 2020	1.74 cm	0.93 cm	1.50 cm	0.77 cm

Table 13: Mean Vectorial distance between model and tide gauges tidal amplitude for EAS6 system and reference literature

Finally, the EAS6 tidal elevation has been compared to the TPXO9 tidal barotropic model solutions and reported in the following table in terms of RMSD.

Tidal Component	Root Mean Square Distances
M2	1.91 cm
S2	1.14 cm
K1	0.42 cm
O1	0.21 cm
N2	0.31 cm
P1	0.21 cm
Q1	0.12 cm
K2	0.44 cm

Table 14: RMSD of vectorial distance between EAS6 tidal amplitudes and the global TPXO tidal solution

IV   SYSTEM'S NOTICEABLE EVENTS, OUTAGES OR CHANGES

Date	Change/Event description	System version	other
8 July 2019 EIS	Updated SST nudging; Included assimilation S3B; Lateral open boundary conditions at the Dardanelles Strait.	EAS4	Time series availability: 01/01/2017 to 30 May 2020
30 March 2020 EIS	Model daily data centred at 12.00 UTC (instead 00:00 UTC).	EAS5	Time series availability: From 01/01/2018
15 Dec 2020 EIS	Upgrade of ECWMF atmospheric forcing to higher spatial and temporal resolution	EAS5	
04 May 2021 EIS	Major change of the modeling system due to inclusion of tides	EAS6	Time series availability: From 01/01/2019
29 November 2021	Time series replaced to use a corrected version of the SST satellite product (SST_MED_SST_L4_NRT_OBSERVATIONS_010_004)	EAS6	Time series availability: From 01/01/2019
14 December 2021	Use of Po river dicharge measurements instead of monthly climatologies	EAS6	Time series availability: From EIS
18 October 2022	Ingestion of Sentinel-6A SLA data	EAS6	Time series availability : From 18 October 2022

V   QUALITY CHANGES SINCE PREVIOUS VERSION

March 2019: From EAS4 to EAS5 system (more details in section 0).

The quality of the product is similar to the one of the previous system.

December 2020: Use of higher spatial and temporal resolution ECMWF atmospheric forcing (more details in section 0).

The quality assessment of the daily analysis physical fields carried out using the higher resolution atmospheric forcing, has provided no significantly changes with respect to the previous system.

May 2021: Inclusion of tides: the tidal potential is calculated across the domain for the 8 major constituents of the Mediterranean Sea: M2, S2, N2, K2, K1, O1, P1, Q1. In addition to this, tidal forcing is applied along the lateral boundaries in the Atlantic Ocean by means of tidal elevation and tidal currents. Reduction of the NEMO time step from 240 to 120 s. Change of model bathymetry. Increased bottom friction at Gibraltar strait. OceanVar scheme has been updated in order to account for the tidal signal in the along-track altimeter observations.

In the following figures we report the main quality changes between new system EAS6 with respect to the previous one EAS5 in terms of time averaged (year 2019) profiles of Temperature (Figure 28, Figure 29) and Salinity (Figure 30, Figure 31) RMSD and bias with respect to in-situ observations as well as daily area averaged time series of SLA with respect to satellite data (Figure 32).

In all comparison we can notice a slight decrease of both RMSD and bias in the new system EAS6 with respect to EAS5.
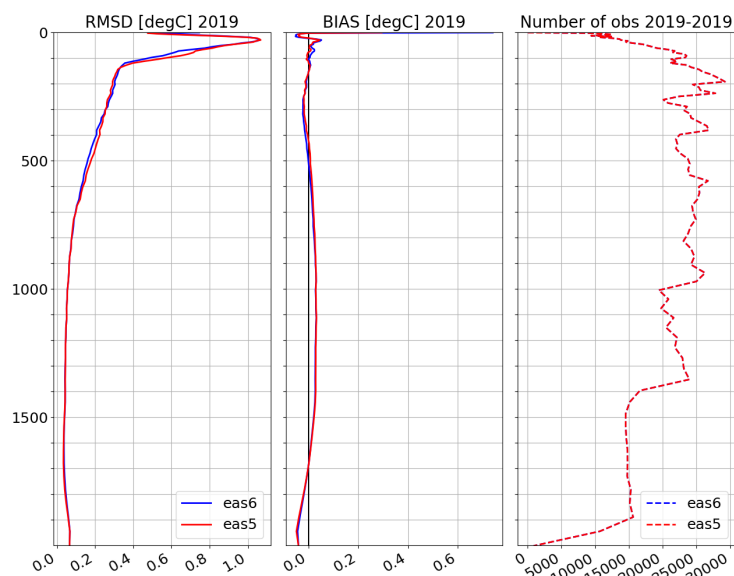

Figure 28: Time averaged (year 2019) profiles (0-2000m) of Temperature RMSD and bias with respect to in-situ observations: EAS5 (red line) and EAS6 (blue line). Right panel represent n. of observations.
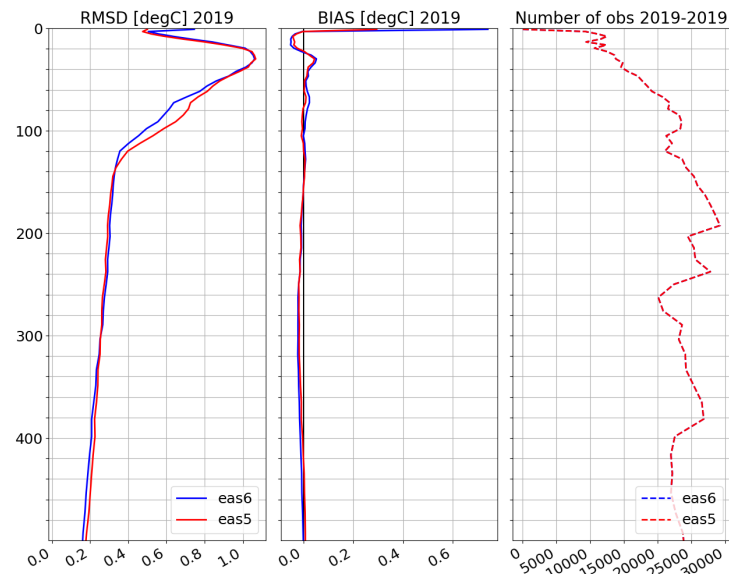
Figure 29: Time averaged (year 2019) profiles (0-500m) of Temperature RMSD and bias with respect to in-situ observations: EAS5 (red line) and EAS6 (blue line). Right panel represent n. of observations.
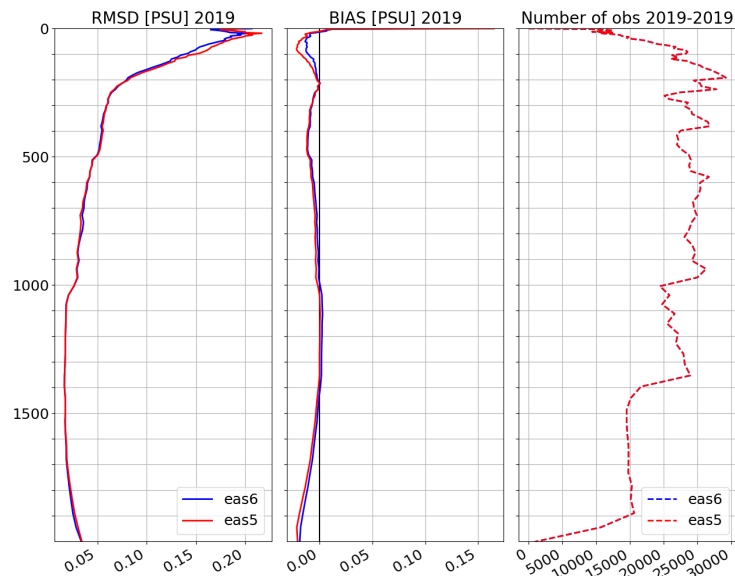

Figure 30: Time averaged (year 2019) profiles (0-2000m) of Salinity RMSD and bias with respect to in-situ observations: EAS5 (red line) and EAS6 (blue line). Right panel represent n. of observations.
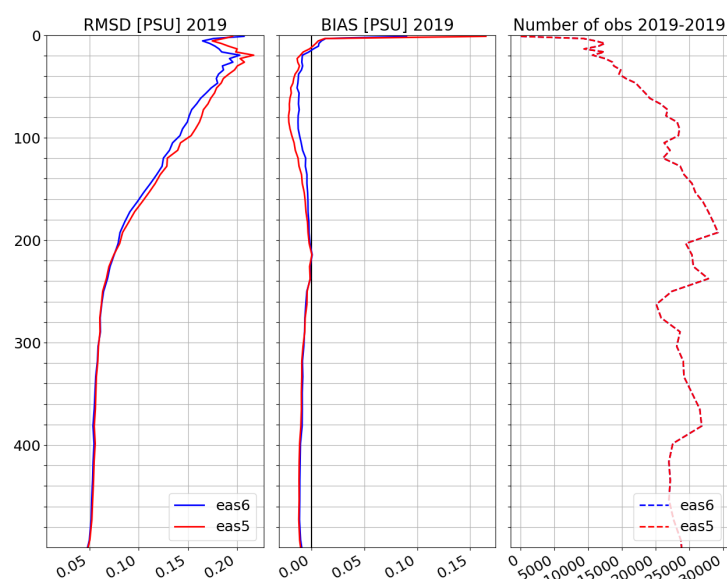
Figure 31: Time averaged (year 2019) profiles (0-500m) of Salinity RMSD and bias with respect to in-situ observations: EAS5 (red line) and EAS6 (blue line). Right panel represent n. of observations.
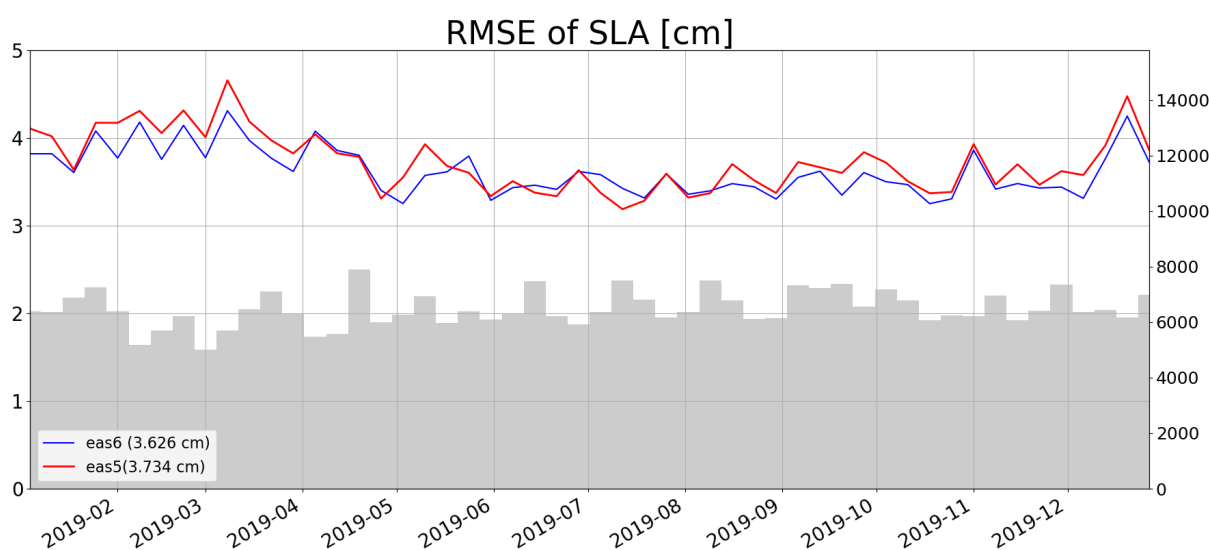

Figure 32: Time series (year 2019) of SLA RMSD with respect to satellite data: EAS5 (red line) and EAS6 (blue line). Grey bars represent n. of observations.

November 2021: Use of a corrected version of the SST L4 satellite product (SST_MED_SST_L4_NRT_OBSERVATIONS_010_004) which was affected by an issue starting from April 2019 and was replaced with a new correct dataset.

An experiment has been done in 2019 to assess the impact of the correction in the satellite SST data on the MEDSEA_ANALYSISFORECAST_PHY_006_013 product.

Figure 33 provides the SST RMSD and Bias of the new and previous model results with respect o satellite L4 data and showing that the mean impact in the whole basin is negligible.
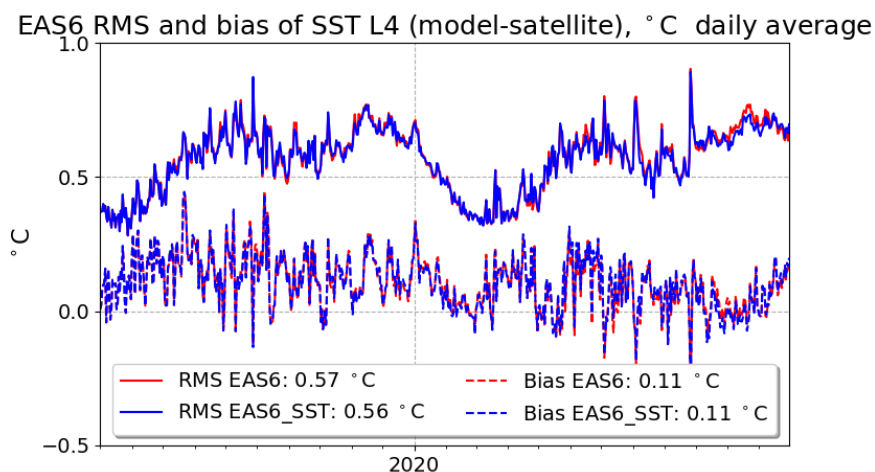
Figure 33: Time series of SST RMSD and Bias of model outputs during year 2019 compared to SST L4 satellite data for an experiment which is relaxed using corrupted data (red lines) and the new experiment using corrected SST data (blue lines).

Figure 34 provides the temperature RMSD along 9 vertical layers averaged in the whole Mediterranean Sea with respect to *insitu* observations and showing a slight decrease of the error when corrected SST data are used to relax the model non solar radiation.
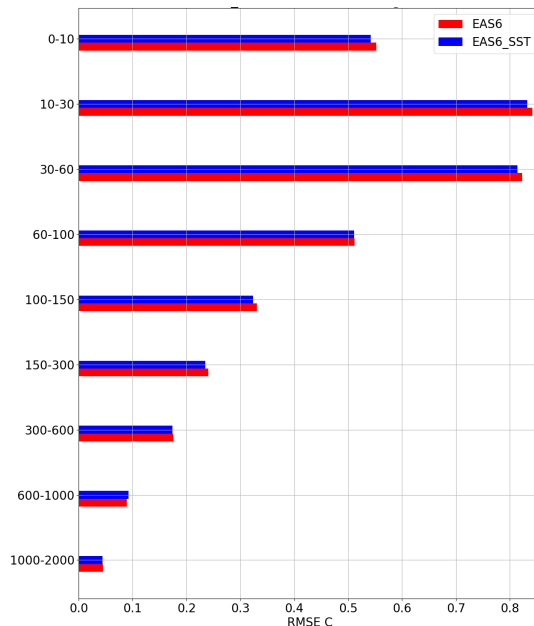

Figure 34: Temperature RMSD along 9 vertical layers: model outputs with respect to insitu observations for the experiment which is relaxed using corrupted data (red lines) and the new experiment using corrected SST data (blue lines).

December 2021: Use of daily Po river discharge measurements distributed by ARPAE (Regional Agency for Prevention, Environment and Energy of Emilia-Romagna, Italy) and available from the website: https://simc.arpae.it/dext3r/. The Po river discharge is measured at the closing point of the drainage basin in Pontelagoscuro. The measured Po river runoff is in average lower than climatological values except for several periods where large discharges were recorded (see Figure 35).
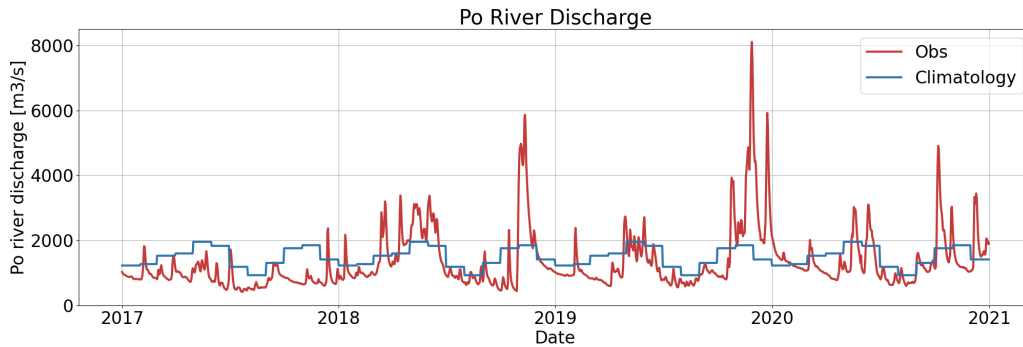

Figure 35: Time series of Po river discharge: daily measurements (red) and monthly climatologies (blue).

The model validation does not provide significant differences when considering yearly statistics in the basin and especially when data assimilation is included. Slight improvements have been achieved when comparing hindcast simulations during flooding events such as November 2018 and November-December 2019.

Figure 36 presents the RMSD (left) and Bias (right) of the model salinity evaluated in the North Adriatic Sea (region 11) during November 2018 showing that the higher frequency Po runoff produces some reduction of the salinity error especially at surface layers.
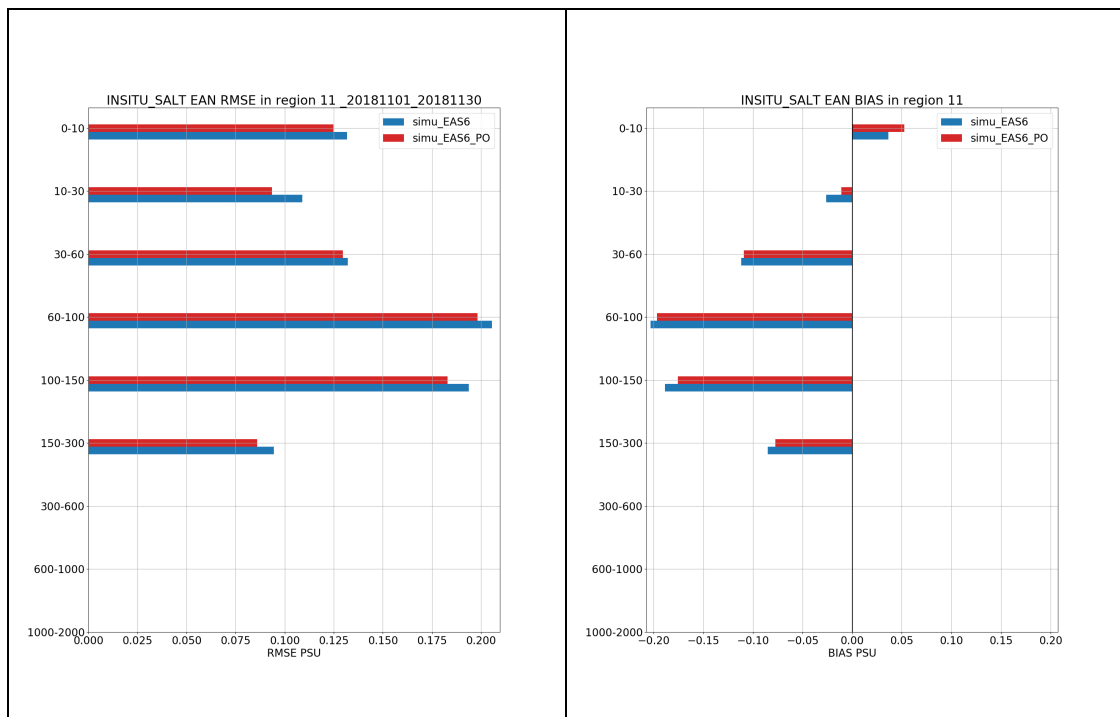

Figure 36. Salinity RMSD (left) and Bias (right) evaluated comparing the daily mean model outputs of the EAS6 experiments forced with Po river climatologies (blue) and with daily observations (red) with respect to *insitu* observations in November 2018 in the North Adriatic Sea (region 11).

Similar results are achieved in the period November-December 2019 (period of large Po river discharge) and presented in Figure 37.

However we should consider that a validation analysis in such a short period and in this small and shallow area is affected by the low availability of *insitu* data.
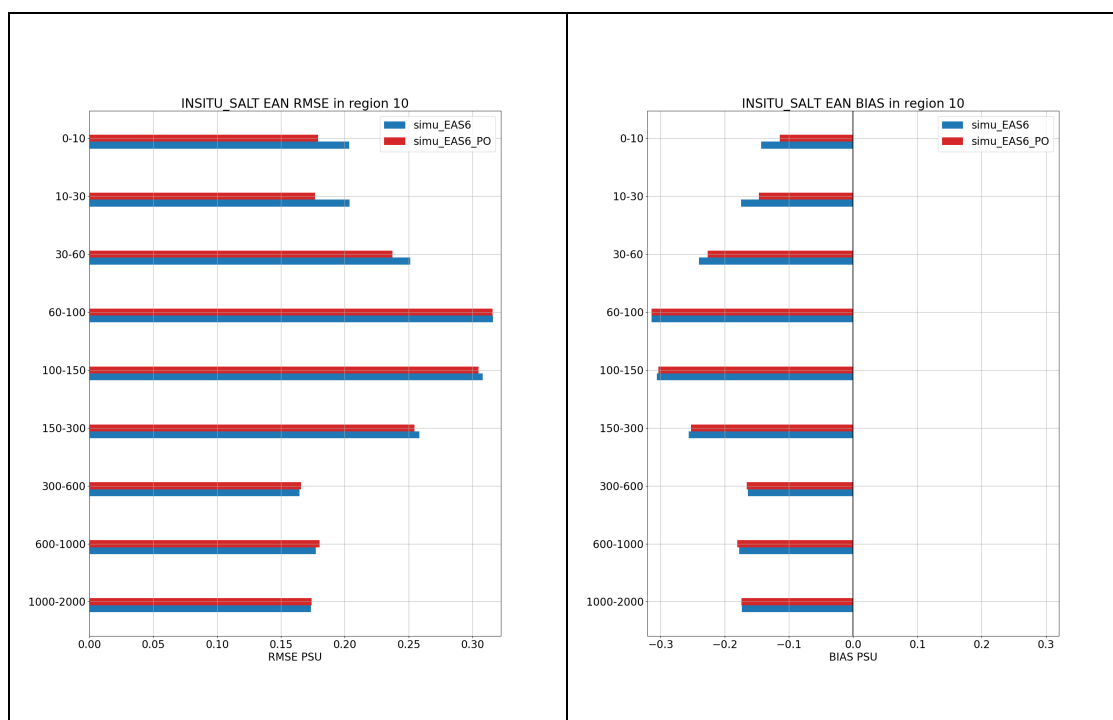

Figure 37. Salinity RMSD (left) and Bias (right) evaluated comparing the daily mean model outputs of the EAS6 experiments forced with Po river climatologies (blue) and with daily observations (red) with respect to insitu observations in November-December 2019 in the South Adriatic Sea (region 10).

October 2022: Ingestion of Sentinel-6A (S6A) Sea Level Anomaly Satellite Altimeter Observations.

The impact of the assimilation of SLA data in the EAS6 system is investigated for the period 28 March - 28 June 2022 (in total three months). The operational system EAS6 has been run with and without the ingestion of SLA observations from S6A, namely EAS6_mfs1_s6a and EAS6_mfs1_nos6a, respectively.

In the following table the mean RMS misfits (known also as innovations) calculated at observation time during the forward model integration (called first guess at appropriate time or FGAT) are provided for SLA, temperature (T) and salinity (S), at different model layers for temperature and salinity (1-15 m, 15-45 m, 45-135 m, 100-200 m, 200-400 m, 400-800 m).

	No Sentinel-6A (EAS6_mfs1_nos6a)		Sentinel-6A (EAS6_mfs1_s6a)	
SLA (cm)	3.1		3.0	
	T (°C)	**S (psu)**	**T (°C)**	**S (psu)**
1-15 m	0.65	0.18	0.67	0.17

15-45 m	0.63	0.16	0.61	0.15
45 - 135 m	0.30	0.12	0.30	0.12
100-200 m	0.22	0.083	0.23	0.085
200 - 400 m	0.20	0.048	0.20	0.049
400 - 800 m	0.11	0.028	0.12	0.029

Table 15: Time and space averaged RMS misfits of SLA with respect to all available satellites and of Temperature and Salinity along 6 vertical layers for the twin experiment with (EAS6_mfs1_s6a) and without (EAS6_mfs1_s6a) assimilation of Sentinel-6A SLA observations.

Figure 38 presents the RMS of SLA misfits between 28 March 2022 and 28 June 2022 for the twin experiments showing a reduced misfit when S6A SLA observations are assimilated. The error evolution of the experiments is close in the first days, since they start from the same initial conditions, while after 2 weeks the assimilation of S6A data produces a reduction of the RMS misfits from 3.1 cm to 3 cm. We note that the amount of data ingested has increased by approximately 20% with the introduction of S6A.
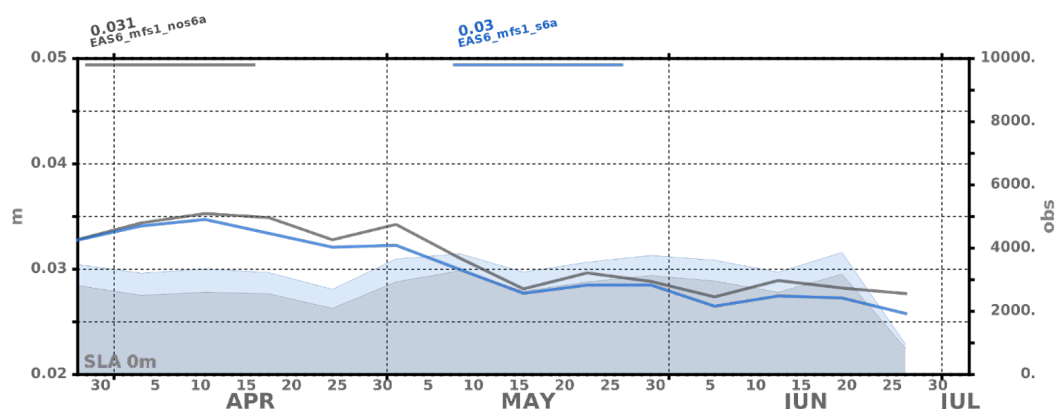

Figure 38. Weekly time series of RMS of SLA misfits between 28 March 2022 and 28 June 2022. The experiment EAS6_mfs1_nos6a without Sentinel-6A assimilation (grey line) and EAS6_mfs1_s6a with Sentinel-6A assimilation (blue) are shown. The time averaged RMS of SLA misfits (m) is printed on the legend. The number of assimilated observations (right y-axis) is shaded with the respective colour.

The analysis shows that the information incorporated with the new dataset is in agreement with the already existing ones and does not degrade the system. There are some improvements at the sampling locations of other satellites as demonstrated by the misfit statistics. The temperature and salinity estimates are also evaluated since they are directly updated by SLA assimilation. First findings reveal differences in temperature and salinity with close error estimates.

VI REFERENCES

Carrere L., F. Lyard, M. Cancet, A. Guillot, N. Picot: FES 2014, a new tidal model – Validation results and perspectives for improvements, presentation to ESA Living Planet Conference, Prague 2016.

Clementi, E., Pistoia, J., Delrosso, D., Mattia, G., Fratianni, C., Storto, A., Ciliberti, S., Lemieux, B., Fenu, E., Simoncelli, S., Drudi, M., Grandi, A., Padeletti, D., Di Pietro, P., Pinardi, N., (2017a). A 1/24 degree resolution Mediterranean analysis and forecast modelling system for the Copernicus Marine Environment Monitoring Service. Extended abstract to the 8th EuroGOOS Conference, Bergen.

Clementi, E., Oddo, P., Drudi, M., Pinardi, N., Korres, G., Grandi A., (2017b). Coupling hydrodynamic and wave models: first step and sensitivity experiments in the Mediterranean Sea. *Ocean Dynamics*. doi: https://doi.org/10.1007/s10236-017-1087-7.

Desroziers, G., Berre, L., Chapnik, B. and Poli, P., (2005). Diagnosis of observation, background and analysis-error statistics in observation space. Q.J.R. Meteorol. Soc. 131: 3385–3396. doi: 10.1256/qj.05.108.

Dobricic Srdjan, and Nadia Pinardi (2008). An oceanographic three-dimensional variational data ssimilation scheme. Ocean Modelling, 22 (3-4) 89-105.

Dobricic, S., Pinardi, N., Adani, M., Tonani, M., Fratianni, C., Bonazzi, A., Fernandez, V., (2007). Daily oceanographic analyses by Mediterranean Forecasting System at the basin scale. Ocean Sci., 3, 149-157.

Dobricic, Srdjan (2005). New mean dynamic topography of the mediterranean calculated fron assimilation system diagnostic. GRL, 32.

Dombrowsky, E., Bertino, L., Brassington, G.B., Chassignet, E.P., Davidson, F., Hurlburt, H.E., Kamachi, M., Lee, T., Martin, M.J., Meu, S., Tonani M., (2009). GODAE Systems in operation, Oceanography, Volume 22-3, 83,95.

Drevillon, M., Bourdalle-Badie, R., Derval, C., Drillet, Y., Lelouche, J. M., Remy, E., Tranchant, B., Benkiran, M., Greiner, E., Guinehut, S., Verbrugge, N., Garric, G., Testut, C. E., Laborie, M., Nouel, L., Bahurel, P., Bricaud, C., Crosnier, L., Dombrosky, E., Durand, E., Ferry, N., Hernandez, F., Le Galloudec, O., Messal, F., Parent, L. (2008). The GODAE/MercatorOcean global ocean forecasting system: results, applications and prospects, J. Operational Oceanogr., 1(1), 51–57.

Estubier A., and Levy M., (2000). Quel schema numerique pour le transport d'organismes biologiques par la circulation oceanique. Note Techniques du Pole de modelisation, Institut Pierre-Simon Laplace, pp 81

Fekete, B. M., Vorosmarty, C. J., Grabs, W., (1999). Global, Composite Runoff Fields Based on Observed River Discharge and Simulated Water Balances, Tech. Rep. 22, Global Runoff Data Cent., Koblenz, Germany.

Flather, R.A. (1976). A tidal model of the northwest European continental shelf. Memories de la Societe Royale des Sciences de Liege 6 (10), 141–164

Gunther, H., Hasselmann, H., Janssen, P.A.E.M., (1993). The WAM model cycle 4, DKRZ report n. 4.

Hasselmann, K. (1974). On the characterization of ocean waves due to white capping, Boundary-Layer Meteorology, 6, 107-127.

Hasselmann, S., and Hasselmann, K. (1985). Computations and parameterizations of the nonlinear energy transfer in a gravity wave spectrum. Part I: A new method for efficient computations of the exact nonlinear transfer integral, J. Phys. Ocean., 15, 1369-1377.

COPERNICUS MARINE ENVIRONMENT MONITORING SERVICE

Hasselmann, S., Hasselmann, K., Allender, J.H., Barnett, T.P., (1985). Computations and parameterizations of the nonlinear energy transfer in a gravity wave spectrum. Part II: Parameterizations of the nonlinear energy transfer for application in wave models, J. Phys. Ocean., 15, 1378-1391.

Houpert, L., Testor, P., Durrieu De Madron, X., (2015). Gridded climatology of the Mixed Layer (Depth and Temperature), the bottom of the Seasonal Thermocline (Depth and Temperature), and the upper-ocean Heat Storage Rate for the Mediterrean Sea. SEANOE. http://doi.org/10.17882/46532

Janssen, P.A.E.M. (1989). Wave induced stress and the drag of air flow over sea wave, J. Phys. Ocean., 19, 745-754.

Janssen, P.A.E.M. (1991). Quasi-Linear theory of wind wave generation applied to wave forecasting, J. Phys. Ocean., 21, 1631-1642.

Komen, G.J., Hasselmann, S., Hasselmann, K., (1984). On the existence of a fully developed windsea spectrum, J. Phys. Ocean., 14, 1271-1285.

Kourafalou, V.H., and Barbopoulos, K., (2003). High resolution simulations on the North Aegean Sea seasonal circulation, Ann. Geophys., 21, 251–265.

Lynch, D.R and W.G. Gray (1979). A wave equation model for finite element tidal computations. In: Computers & fluids 7.3, pp. 207–228.

Maraldi C., Chanut, J., Levier, B., Ayoub, N., De Mey, P., Reffray, G., Lyard, F., Cailleau, S., Drévillon, M., Fanjul, E.A., Sotillo, M.G., Marsaleix, P., and the Mercator Research and Development Team (2013). NEMO on the shelf: assessment of the Iberia–Biscay–Ireland configuration. Ocean Sci., 9, 745–771.

Madec, G. and the NEMO system Team. NEMO Ocean Engine, Scientific Notes of Climate Modelling Center (27) - ISSN 1288-1619, Institut Pierre-Simon Laplace (IPSL) 2019, http://doi.org/10.5281/zenodo.1464816.

Maderich V., Ilyin Y., Lemeshko E., 2015. Seasonal and interannual variability of the water exchange in the Turkish Straits System estimated by modelling. Mediterranean Marine Science, [S.l.], v. 16, n. 2, p. 444-459, ISSN 1791-6763, doi:http://dx.doi.org/10.12681/mms.1103.

Marchesiello, P., McWilliams, J. C., Shchepetkin, A., (2001). Open boundary conditions for long-term integration of regional oceanic models. Ocean modelling, 3(1), 1-20.

Oddo, P., Adani, M., Pinardi, N., Fratianni, C., Tonani, M., Pettenuzzo, D., (2009). A Nested Atlantic-Mediterranean Sea General Circulation Model for Operational Forecasting. Ocean Sci. Discuss., 6, 1093-1127.

Oddo, P., Bonaduce, A., Pinardi, N., Guarnieri, A., (2014) Sensitivity of the Mediterranean sea level to atmospheric pressure and free surface elevation numerical formulation in NEMO. Geosci. Model Dev., 7, 3001–3015.

Palma M.et al. (2020). Short-term, linear, and non-linear local effects of the tides on the surface dynamics in a new, high-resolution model of the Mediterranean Sea circulation. Ocean Dynamics, 70. DOI: 10.1007/s10236-020-01364-6

Pinardi, N., Allen, I., De Mey, P., Korres, G., Lascaratos, A., Le Traon, P.Y., Maillard, C., Manzella G., Tziavos, C., (2003). The Mediterranean ocean Forecasting System: first phase of implementation (1998-2001). Ann. Geophys., 21, 1, 3-20.

Pistoia, J., Clementi, E., Delrosso, D., Mattia, G., Fratianni, C., Drudi, M., Grandi, A., Padeletti, D., Di Pietro, P., Storto, A., Pinardi., N., (2017). Last improvements in the data assimilation scheme for the

Mediterranean Analysis and Forecast system of the Copernicus Marine Service. Extended abstract to the 8th EuroGOOS Conference, Bergen.

Pacanowsky, R.C., and Philander S.G.H., (1981) Parameterization of vertical mixing in numerical models of tropical oceans. J Phys Oceanogr 11:1443-1451

Pettenuzzo, D., Large, W.G., Pinardi, N., (2010) On the corrections of ERA-40 surface flux products consistent with the Mediterranean heat and water budgets and the connection between basin surface total heat flux and NAO. Journal of Geophysical Research 115, C06022, doi:10.1029/2009JC005631

Provini, A., Crosa, G., Marchetti, R., (1992). Nutrient export from Po and Adige river basins over the last 20 years. Sci. Total Environ; suppl.: 291-313

Raicich, F. (1996). On fresh water balance of the Adriatic Sea, J. Mar. Syst., 9, 305–319.

Rio, M.-H., Pascual, A., Poulain, P.-M., Menna, M., Barceló, B., Tintoré, J., (2014). Computation of a new mean dynamic topography for the Mediterranean Sea from model outputs, altimeter measurements and oceanographic in situ data. Ocean Science, 10, 731-744.

Roullet, G., and Madec G., (2000). Salt conservation, free surface, and varying levels: a new formulation for ocean general circulation models. J.G.R., 105, C10, 23,927-23,942.

Soto-Navaro, J., Criado-Aldeanueva, F., Garci-Lafuente, J., Sanchez-Roman, A., (2010). Estimation of the Atlantic inflow through the Strait of Gibraltar from climatological and in situ data. J. Jeophysics Research, 10.1029/2010JC006302

Storto, A., Masina, S., Navarra, A., (2015). Evaluation of the CMCC eddy-permitting global ocean physical reanalysis system (C-GLORS, 1982-2012) and its assimilation components. *Quarterly Journal of the Royal Meteorological Society*, 142, 738–758, doi: 10.1002/qj.2673.

Tolman H.L. (2009). User Manual and system documentation of WAVEWATCH III version 3.14. NOAA/NWS/NCEP/MMAB Technical Note 276, 194 pp + Appendices.

Tolman H.L. (2002). Validation of WAVEWATCH III version 1.15 for a global domain.NOAA / NWS / NCEP / OMB Technical Note 213, 33 pp.

Tonani, M., Balmaseda, M., Bertino, L., Blockley, E., Brassington, G., Davidson, F., Drillet, Y., Hogan, P., Kuragano, T., Lee, T., Mehra, A., Paranathara, F., Tanajura, CAS, Wang, H., (2015) Status and future of global and regional ocean prediction systems. J Operational Oceanography 8:201-220, doi:10.1080/1755876X.2015.1049892.

Tonani, M., Teruzzi, A., Korres, G., Pinardi, N., Crise, A., Adani, M., Oddo, P., Dobricic, S., Fratianni, C., Drudi, M., Salon, S., Grandi, A., Girardi, G., Lyubartsev, V., Marino, S., (2014). The Mediterranean Monitoring and Forecasting Centre, a component of the MyOcean system. Proceedings of the 6th Int. Conference on EuroGOOS 4-6 October 2011, Sopot, Poland. Edited by H. Dahlin, N.C. Fleming and S. E. Petersson. First published 2014. Eurogoos Publication no. 30. ISBN 978-91-974828-9-9.

Tonani, M., Pinardi, N., Dobricic, S., Pujol, I., Fratianni, C., (2008). A high-resolution free-surface model of the Mediterranean Sea. Ocean Sci., 4, 1-14.

Tonani, M., Simoncelli, S., Grandi, A., Pinardi, N., (2013). New gridded climatologies, from in-situ observations, for the Mediterranean Sea. Abstract to IMDIS 2013. http://www.google.it/url?sa=t&rct=j&q=&esrc=s&source=web&cd=2&ved=0ahUKEwiss_HHm_XLAhU CdQ8KHXR1AQ4QFggjMAE&url=http%3A%2F%2Fimdis2013.seadatanet.org%2Fcontent%2Fdownload %2F93851%2F1140805%2Ffile%2FSDN2_D64_WP6_IMDIS2013_proceedings_abstracts.pdf&usg=AFQj CNHnDVXHRCMlaEVd0p7RafnWwWIi0w&bvm=bv.118443451,d.ZWU

Tsimplis, M.N., Proctor, R., Flather, R. A. (1995). Two-dimensional tidal model for the Mediterranean Sea. J. of Geophysical Research. https://doi.org/10.1029/95JC01671

Van Leer, B. (1979) Towards the Ultimate Conservative Difference Scheme, V. A Second Order Sequel to Godunov's Method. J Comp Phys 32:101-136